Parkinson's-Linked Synaptojanin 1 Loss in Dopamine Neurons Triggers Synaptic Degeneration and Striatal TH Interneuron Compensation

Bandhan Mukherjee[1,#], Youneng Lin[1,#], Man Liu[1,&], Zhaoyan Li[1, &], Xiaoxing Cao[1], and Mian Cao[1,2*]

1. Programme in Neuroscience and Behavioural Disorders, Duke-NUS Medical School, Singapore

2. Department of Physiology, National University of Singapore, Singapore

#,&: These authors contributed equally

* Corresponding Author

Contact Information: mian.cao@duke-nus.edu.sg

Abstract

Synaptic dysfunction is increasingly recognized as an early hallmark of Parkinson's disease (PD). Synaptojanin 1 (SJ1), a synaptic phosphoinositide phosphatase essential for synaptic vesicle recycling, is genetically linked to early-onset Parkinsonism (EOP). While germline SJ1 knockout mice are perinatal lethal, SJ1-R258Q knock-in mice recapitulate EOP-like symptoms and exhibit selective dystrophy of nigrostriatal dopamine (DA) terminals. However, these whole-body mutants limit understanding of SJ1's role in the DA system. Here, we generated DA neuron-specific SJ1 conditional KO (SJ1-DA cKO) mice. Complete SJ1 loss caused severe synaptic dystrophy throughout the striatum, indicating a cell-autonomous role of SJ1 in both substantia nigra and ventral tegmental area DA subtypes. Surprisingly, despite profound synaptic degeneration and DA deficiency, SJ1-DA cKO mice showed no overt motor deficits. Instead, we observed a robust induction of striatal tyrosine hydroxylase-positive interneurons (iTHINs), which expressed multiple DA markers and formed new connections with degenerating DA terminals, suggesting a potential local compensation. In contrast, acute SJ1 deletion in adult/aged DA neurons caused similar terminal pathology but limited iTHINs induction. Together, our findings reveal a critical role for SJ1 in maintaining DA synaptic function and uncover an adaptive striatal response to DA loss, offering insights into compensatory mechanisms relevant to PD pathogenesis.

Key words: Synaptojanin1; DA conditional KO mice; synaptic degeneration; tyrosine hydroxylase-positive interneurons; striatal adaptive compensation; Parkinson's disease

Introduction

Parkinson's disease (PD) is the second most common neurodegenerative disorder, primarily affecting movement. The pathological hallmarks of PD include the selective loss of dopamine (DA) neurons in the substantia nigra pars compacta (SNc) and DA deficiency in the striatum.

Although over 90% of PD cases are sporadic, recent genetic studies have identified more than 20 risk genes and 90 genomic risk loci associated with both familial and sporadic PD[1]. Several of these genes regulate endocytic trafficking at presynaptic terminals, suggesting that impaired synaptic vesicle (SV) recycling is an early pathological feature of PD[2]. A major SV recycling pathway involves clathrin-mediated endocytosis (CME), in which Synaptojanin 1 (SJ1), a lipid phosphatase, plays a crucial role[3]. SJ1 facilitates clathrin uncoating by dephosphorylating $PI(4,5)P_2$ on the plasma membrane and releasing clathrin adaptors. In its absence, clathrin-coated vesicles (CCVs) accumulate at synapses, as demonstrated in multiple model organisms[4-7].

A homozygous missense mutation (R258Q) in SJ1 has been previously identified in early-onset Parkinsonism (EOP), establishing SJ1 as the PARK20 gene[8,9]. This mutation inactivates the Sac phosphatase domain, resulting in partial loss-of-function (LOF). Since then, additional SJ1 mutations have been linked to Parkinsonism and epilepsy, most of which are homozygous missense or nonsense mutations[2,10]. A strong genotype-phenotype correlation exists, where nonsense mutations causing premature truncation in the homozygous state led to severe neurodegeneration, seizures, and early mortality[11]. In contrast, homozygous or compound heterozygous missense mutations are associated with milder phenotypes, including Parkinsonism and seizure susceptibility[10,12].

More recently, rare heterozygous SJ1 variants have been implicated in EOP, and Sac domain variants have been linked to sporadic PD[13]. Additionally, a novel expression quantitative trait locus (eQTL) connection between rs10847864 and SJ1 was identified, highlighting convergence between familial and GWAS studies[14]. Furthermore, SJ1 expression is reduced in blood and postmortem PD brain tissues, suggesting it may serve as a biomarker for sporadic PD[15].

Multiple mouse models have been developed to study SJ1 LOF. Complete SJ1 loss in constitutive homozygous knockout (KO) mice results in early mortality and severe epilepsy, mirroring human patients with homozygous nonsense mutations[11,16]. Aged SJ1-haploinsufficient (+/-) mice show PD-like features, including alpha-synuclein accumulation,

72 autophagy defects, and DA terminal degeneration[17]. They also exhibit impaired astrocytic
73 glucose sensing and lysosomal dysfunction in midbrain neurons[18,19].

74 Our previously generated SJ1 knock-in (KI) mice carrying the R258Q mutation (SJ1-KI^{RQ})
75 exhibit neurological symptoms reminiscent of EOP, including early-onset epilepsy and motor
76 coordination deficits[20]. These mice display generalized synaptic endocytic defects and
77 selective synaptic degeneration in a subset of DA neurons in nigrostriatal pathway, a hallmark
78 of PD pathology[20]. Additionally, we demonstrated a synergistic interaction between SJ1 and
79 auxilin (PARK19), another PD-linked clathrin uncoating protein[21]. Auxilin-KO mice exhibit
80 dystrophic nigrostriatal DA terminals similar to SJ1-KI^{RQ} mice. In double mutant (Aux-KO/SJ1-
81 KI^{RQ}) mice, lifespan is dramatically reduced, and synaptic endocytic defects and striatal
82 dystrophic changes are exacerbated, further supporting the vulnerability of nigrostriatal
83 neurons to synaptic endocytic impairments[21].

84 Synergistic effects of SJ1 with other PD-linked proteins have also been demonstrated in
85 double mutant mouse models. INPP5F/Sac2, a PI4P phosphatase involved in endosomal
86 trafficking, has been identified as a PD risk gene through GWAS[22]. Sac2-KO/ SJ1-KI^{RQ} mice
87 show shortened lifespan, more severe endocytic defects, and earlier DA terminal dystrophy[23].
88 In addition, combining SJ1 heterozygosity with LRRK2 G2019S worsens DA release deficits
89 and motor impairments in aged mice[24].

90 While these mouse models have provided valuable insights into SJ1 function in PD, they are
91 all constitutive whole-body mutants, leading to complex behavioral phenotypes and even early
92 death due to global SJ1 loss in the brain. To better delineate SJ1's role in DA neurons in PD,
93 we generated novel DA neuron-specific SJ1 conditional KO models (both genetic and acute
94 deletions) in this study. Complete SJ1 loss in DA neurons results in severe DA terminal
95 dystrophy and DA deficiency throughout the striatum, but surprisingly, no overt motor deficits.
96 Instead, we observed a robust compensatory increase in striatal tyrosine hydroxylase-positive
97 interneurons (THINs). These induced THINs acquire DA-like properties and form new
98 connections with DA terminals, potentially compensating for DA loss. Our study not only
99 reinforces the critical role of SJ1 in DA synaptic transmission but also reveals a novel
100 compensatory mechanism, which if pharmacologically enhanced, might delay or mitigate PD.

101 **Results**

102 **Generation of DA-specific SJ1 conditional knockout (cKO) mice genetically**

103 Given that conventional SJ1 KO mice exhibit perinatal lethality within 24 hours of birth, we
104 generated SJ1 flx/flx mice by inserting loxP sites flanking exon 4 of *Synj1* gene using
105 CRISPR/Cas9. These mice were then crossed with the DAT-IRES-Cre line to create DA-
106 specific SJ1 conditional KO mice (DAT-Cre;SJ1 flx/flx), hereafter referred to as SJ1 cKO^{DAT}
107 (Figures 1A and S1A).

108 To confirm successful recombination, we performed immunohistochemistry (IHC) on fixed
109 frozen brain sections using antibodies against SJ1 and DA marker tyrosine hydroxylase (TH).
110 In SJ1 cKO^{DAT} mice, SJ1 protein was selectively depleted in TH-positive DA neurons in the
111 SNc and ventral tegmental area (VTA), while SJ1 expression in TH-negative neurons and non-
112 DA brain regions, such as the hippocampus, remained intact (Figure 1B). These findings
113 confirm efficient and specific KO of SJ1 in DA neurons. SJ1 cKO^{DAT} mice survived into
114 adulthood without seizures, suggesting that epilepsy reported in SJ1-KI^{RQ} mice and
115 constitutive SJ1 KO mice is likely due to SJ1 loss in other brain regions, such as the
116 hippocampus and cortex[16,20].

117 **DA Terminal Pathology and DA Deficiency in the SJ1 cKO^{DAT} Striatum**

118 To investigate DA-specific pathology in SJ1 cKO^{DAT} mice, we performed IHC for DA-related
119 markers in both midbrain (DA soma) and striatum (DA terminals). In the midbrain, TH-positive
120 DA neurons appeared morphologically intact, with no significant loss of DA neurons in either
121 the SNc or VTA at 2-3 months old and 6-8 months old (Figure S1B). However, in the striatum,
122 we observed numerous dopamine transporter (DAT) positive dystrophic clusters in SJ1
123 cKO^{DAT} but not in the control (Figures 1C and 1D). In line with our previous study[20,21], this
124 striatal pathology emerged as early as three weeks after birth, progressively increasing in size
125 and number, and peaking at 2–3 months of age (Figure S1E). Importantly, SJ1 cKO^{DAT} mice
126 exhibited this pathology throughout the striatum, including the dorsal and ventral striatum
127 (Figures 1C and S1C). This differs from the previously reported SJ1-KI^{RQ} mice[20], where
128 dystrophic DA terminals were primarily restricted to the dorsal striatum (nigrostriatal pathway)
129 (Figure S1D). This widespread pathology observed in the striatum suggests that the complete
130 loss of SJ1 impacted both SNc and VTA DA neurons. Together, the results from SJ1-KI^{RQ} and
131 SJ1 cKO^{DAT} mice indicate that the loss of SJ1 in DA neurons is sufficient to cause DA terminal
132 dystrophy in a cell-autonomous and gene-dosage dependent manner.

133 As shown in Figures 1E and S2A, these dystrophic clusters were immunopositive for several
134 other DA markers, including TH, aromatic L-amino acid decarboxylase (AADC), vesicular
135 monoamine transporter 2 (vMAT2), and synaptic vesicle glycoprotein 2C (SV2C). Additional
136 analyses revealed partial colocalization of these DAT-positive clusters with general synaptic

137 markers such as synaptotagmin-1 (Syt1) and α-synuclein (Figures S2B and S2C). In contrast,
138 the pathological form of α-synuclein (pSer129-α-syn) was not detected in these clusters
139 (Figure S2D). Moreover, these dystrophic clusters lacked colocalization with D2 dopamine
140 receptors (D2R) or the medium spiny neuron (MSN) marker Darpp32, indicating that the
141 pathology is restricted to DA terminals (Figures S2E and S2F). Additionally, immunostaining
142 with microglial marker, ionized calcium-binding adapter molecule (Iba1), and astrocyte marker,
143 glial fibrillary acidic protein (GFAP), did not show any obvious gliosis and inflammation in the
144 striatum (Figures S2G and S2H). Interestingly, these clusters were negative for clathrin-
145 dependent endocytic proteins either (e.g., clathrin light chain, endophilin 1, and amphiphysin
146 1), suggesting a clathrin-independent mechanism may underlie DA terminal dystrophy
147 (Figures S3A-S3D). Indeed, electron microscopy (EM) of the SJ1 cKO^{DAT} striatum revealed
148 multilayered, whirl-like membrane structures, similar to those previously observed in SJ1-KI^{RQ}
149 and Auxilin-KO mutant mouse models (Figure 1F)[21]. These membrane accumulations
150 correlate with DA marker protein clusters and likely reflect abnormal plasma membrane
151 invaginations at DA terminals. They envelop various organelles, including SVs, mitochondria,
152 autophagosomes, and endo/lysosomes; however, clathrin-coated vesicle (CCV) accumulation
153 was not observed (Figures 1F and S4A-S4B).

154 We further performed western blot analysis to assess potential changes in DA-related and
155 synaptic/endocytic protein levels in striatal tissue. SJ1 cKO^{DAT} mice showed a significant
156 reduction in DAT and vMAT2, while TH and AADC levels remained unchanged, indicating
157 impaired presynaptic DA transmission (Figures 2A and 2B). Levels of clathrin-associated
158 endocytic proteins—including SJ1, BIN1, endophilin 1, dynamin, and AP2—were unaffected
159 (Figures S5A and S5B).

160 To assess DA metabolism and homeostasis, we conducted high-performance liquid
161 chromatography (HPLC) on striatal extracts. DA levels were significantly reduced in SJ1
162 cKO^{DAT} mice at both 2–3 and 6–8 months of age (Figure 2C), indicating striatal DA deficiency.
163 Concurrently, elevated levels of DA metabolites DOPAC (not significant) and HVA suggest
164 increased DA degradation, likely resulting from impaired SV recycling, reduced vesicular
165 sequestration, and cytosolic DA buildup (Figure 2C).

166 **No Apparent Motor Coordination Deficits in SJ1 cKO^{DAT} Mice**

167 The strong DA terminal pathology and DA deficiency prompted us to examine the motor
168 function of SJ1 cKO^{DAT} mice. In the open field test, the 2-3 months old SJ1 cKO^{DAT} mice
169 performed equally well compared to control mice, while 6-8 months old SJ1 cKO^{DAT} mice
170 showed reduced total distance and center distance, suggesting their locomotion or exploratory

171 activity is gradually reduced during aging (Figures 2E and 2F). We further performed more
172 specific motor coordination tests: rotarod test and balanced beam test. Surprisingly, unlike
173 SJ1-KI^{RQ} mice which showed strong motor deficits[20], we did not observe obvious motor
174 coordination deficit in SJ1 cKO^{DAT} mice when tested for rotarod and balance beam at either 2-
175 3 months or 6-8 months old (Figures 2G and 2H). These results indicate either the DA terminal
176 pathology observed is not severe enough to impair basic motor function, or compensatory
177 mechanisms may have mitigated DA deficiency.

178 **Locally Adaptive induced TH-positive Interneurons (iTHINs) in SJ1 cKO^{DAT} Striatum**

179 In addition to the TH/DAT-positive dystrophic clusters in DA terminals, we observed a marked
180 increase in TH-positive neurons within the striatum of SJ1 cKO^{DAT} mice (Figure 3A). Striatal
181 TH-positive neurons have been reported in rodents[25-27], primates[28,29], and humans[30-32]..
182 Previous studies using TH-EGFP mice identified them as TH-positive interneurons (THINs),
183 typically undetectable by IHC in wild-type (WT) mice due to low TH expression masked by
184 dense DA axons[33]. In SJ1 cKO^{DAT} mice, however, the strong TH protein signal led us to define
185 them as induced TH-positive interneurons (iTHINs). These iTHINs appeared in both dorsal
186 and ventral striatum (Figure S6A), reaching ~200 per coronal section (Figure 3B). Their
187 emergence paralleled DA terminal dystrophy—first detectable at 3 weeks, peaking at 2–3
188 months, and persisting into adulthood and aging (Figure S6B). Given that SJ1 deletion is
189 restricted to midbrain DA neurons, this suggests a robust and sustained local adaptation in
190 the striatum.

191 In the striatum, 95% of neurons are MSNs. In addition, there are several other striatal
192 interneurons, including neuropeptide Y (NPY), parvalburmin (PV), Calretinin-positive GABA
193 interneurons and choline acetyltransferase (ChAT)-positive cholinergic interneurons[34]. To
194 determine the identity of iTHINs, we performed double staining of TH with specific markers for
195 different neuronal types. As shown in Figure S7A-S7C, iTHINs were not positive for NPY, PV,
196 and ChAT, suggesting they represent a distinct subtype of interneurons. We observed few
197 iTHINs occasionally expressed Calretinin or Darpp32 (Figures S7D and S7E), which is
198 consistent with previous studies and suggest heterogeneity within this population[35,36]. In
199 addition, we don't see obvious changes of other neuronal types we examined in terms of their
200 number, distribution and marker expression levels. Together, these results further support the
201 specificity of iTHINs induction in response to DA terminal pathology**.**

202 **DA-Like Properties of iTHINs in SJ1 cKO^{DAT} Striatum**

203 To investigate whether iTHINs adopt DA-like properties to compensate for DA deficiency, we
204 first assessed their expression of key biosynthetic enzymes. Importantly, in addition to TH,
205 which is the first enzyme to convert L-tyrosine to L-DOPA, we also observed co-expression of
206 the second enzyme AADC, which further converts L-DOPA to DA. All iTHINs were positive for
207 both TH and AADC, suggesting they can potentially produce DA (Figure 3C).

208 We next examined the expression of DA transporters: vMAT2 and DAT, which are required for
209 vesicular packaging and reuptake of DA, respectively. Both markers colocalized with TH-
210 positive clusters at dystrophic DA terminals (Figures 3D and 3E) but were absent from iTHINs
211 somata—although DAT gene promoter activity was detected in these cells (see Figure 5E).

212 Given the known heterogeneity of striatal THINs[34,37], we explored whether iTHINs exhibit
213 subregional adaptations linked to specific midbrain DA neuron subtypes. We first examined
214 aldehyde dehydrogenase 1A1 (ALDH1A1), a marker of A9 SNc DA neurons—the population
215 most vulnerable in PD[38]. As expected, ALDH1A1 labeled ventral-tier SNc neurons in both
216 control and SJ1 cKO^{DAT} mice (Figure S8A). In the striatum, ALDH1A1-positive fibers
217 aggregated with TH/DAT-positive clusters in the dorsal region of SJ1 cKO^{DAT} mice (Figures 3F
218 and S8B), indicating dystrophic changes in A9-derived terminals. Notably, iTHINs in this region
219 also expressed ALDH1A1 protein, whereas those in the ventral striatum did not, suggesting
220 region-specific adaptation (Figures 3G and S8B). We also examined Calbindin, a marker of
221 A10 VTA DA neurons[39]. While Calbindin labeled a subset of TH-positive neurons in the VTA
222 (Figure S8C), it was not expressed in any iTHINs (Figure S8D). Together, these results show
223 that a subset of iTHINs—particularly in the dorsal striatum—exhibit A9-like molecular feature,
224 potentially reflecting a circuit-specific compensatory response to selective nigrostriatal
225 terminal pathology.

226 **A Second Genetic SJ1 cKO Model (SJ1 cKOTH) Recapitulates DA Terminal Pathology**
227 **and iTHINs Adaptation**

228 To validate our findings, we generated an independent cell type-specific KO model by crossing
229 SJ1 flx/flx mice with the TH-IRES-Cre line, obtaining SJ1 cKOTH mice (Figure 4A). While this
230 Cre line also targets TH-positive neurons in other regions (e.g., norepinephrine neurons in the
231 locus coeruleus), our analysis focused on DA neurons in the ventral midbrain and striatum.

232 As shown in Figure 4B, SJ1 was selectively and completely depleted in TH-positive DA
233 neurons of the SNc and VTA. No obvious DA soma loss was observed in the midbrain of 2-3
234 months old mice. However, DA terminals in the striatum displayed the same hallmark
235 pathology seen in SJ1 cKO^{DAT} mice—early-onset (1–2 months) dystrophic clusters positive

236 for DA markers including TH, AADC, DAT, vMAT2, SV2C, and ALDH1A1 (Figures 4C–4F).
237 These clusters were broadly distributed across the striatum, with ALDH1A1 selectively
238 labeling clusters in the dorsal region (Figure 4G), further confirming both SNc and VTA DA
239 neurons were affected due to complete loss of SJ1. Importantly, iTHINs were again robustly
240 induced in the striatum, paralleling DA terminal pathology. These iTHINs co-expressed TH
241 and AADC, with dorsal striatal subsets also expressing ALDH1A1 (Figures 4G and 4H),
242 indicating their DA-like phenotype.

243 Together, results from both SJ1 cKO^{DAT} and cKOTH models demonstrate that SJ1 loss in DA
244 neurons induces cell-autonomous synaptic pathology, which in turn triggers a secondary, non-
245 cell-autonomous compensatory response via local iTHINs.

246 **iTHINs Derive from a pre-existing pool of WT THINs and activate DAT gene expression**
247 **in response to SJ1 loss**

248 To test whether striatal iTHINs in SJ1 cKO models originate from a pre-existing population of
249 THINs, we genetically labeled original THINs by crossing Ai9 reporter mice (Cre-dependent
250 tdTomato expression) with SJ1 cKOTH mice, generating Ai9;SJ1 cKOTH animals (Figure 5A).
251 This enables tdTomato (tdT) expression in all TH gene expressing cells, including DA neurons
252 in the midbrain and THINs in the striatum. As expected, tdT-expressing neurons in the
253 midbrain colocalized with TH immunostaining (Figure 5B). In the striatum, we observed
254 numerous tdT-expressing neurons in both Ai9;TH-Cre (control) and Ai9;SJ1 cKOTH mice,
255 representing the total THINs (Figure 5C). Consistent with prior studies[27], these tdT-expressing
256 striatal neurons in control mice were not positive for anti-TH staining, indicating that they
257 lacked TH protein (Figure 5C). In contrast, all iTHINs (TH-positive) in SJ1 cKOTH mice
258 colocalized with tdT, comprising approximately 30% of total tdT-expressing neurons (Figures
259 5C and 5D). This supports the idea that a subset of WT THINs were induced to express DA-
260 related proteins following SJ1 loss.

261 We further examined the Cre-dependent tdT labeling pattern in Ai9;SJ1 cKO^{DAT} mice with its
262 respective control, Ai9;DAT-Cre (Figure 5A). As expected, DAT-Cre drove tdT labeling in
263 midbrain DA soma and striatal axons in both control and mutant mice (Figures 5E and 5F). In
264 control striatum (Ai9;DAT-Cre), only DA axons were labeled, confirming that WT THINs do not
265 normally express DAT gene. However, in Ai9;SJ1 cKO^{DAT} mice, we unexpectedly observed
266 tdT-expressing cell bodies in the striatum (Figure 5F). Importantly, almost all tdT-expressing
267 neurons were TH-positive, indicating that DAT gene promoter is activated in iTHINs (Figure
268 5G). Despite this, DAT protein was not detected, possibly due to post-transcriptional

269 suppression. These findings reinforce the DA-like identity of iTHINs and reveal their
270 transcriptional adaptability to DA neuron dysfunction.

271 **iTHINs Establish Novel Connectivity with DA Terminals in SJ1 cKO Striatum**

272 To further investigate potential interactions between DA neurons and iTHINs, we employed
273 an AAV-based strategy to locally label DA neurons in the ventral midbrain using a Cre-
274 dependent system. We unilaterally injected AAV5-flex-tdTomato into the ventral midbrain of
275 SJ1 cKOTH, SJ1 cKO^{DAT} and respective Cre line controls, TH-Cre and DAT-Cre (Figure 6A).
276 Four weeks post-injection, we performed TH immunostaining on midbrain and striatum
277 sections to visualize DA neurons and their projections.

278 In both SJ1 cKO and control mice, tdT expression was detected in DA soma (midbrain) and
279 DA fibers (striatum), confirming successful AAV-mediated expression and diffusion throughout
280 DA neurons (Figures 6B-6C). Surprisingly, in SJ1 cKOTH and SJ1 cKO^{DAT} mice, we observed
281 a subset of iTHINs (anti-TH positive) also strongly expressed tdT in the striatum (Figure 6C).
282 Particularly in SJ1 cKOTH mice, despite TH-Cre driving recombination in all THINs, tdT
283 expression was exclusively found in iTHINs (Figures 6C and 6D). In contrast, when AAV5-
284 flex-tdTomato was directly injected into the striatum of SJ1 cKOTH mice, both iTHINs and
285 original WT THINs (anti-TH negative) were randomly labeled (Figures S9A and S9B 2nd row).
286 As in other controls, striatal AAV injection labeled WT THINs in TH-Cre but not DAT-Cre mice,
287 and labeled iTHINs specifically in SJ1 cKO^{DAT} mice (Figures S9B). These results suggest the
288 presence of a newly formed and specific connection between DA neurons and iTHINs, which
289 may allow long-distance material transfer, such as AAV axonal transport and inter-neuronal
290 spreading.

291 To further trace the connectivity between DA neurons and iTHINs, we used a Cre-independent
292 AAV strategy by injecting AAV9-TH-EGFP into the midbrain of B6 control and SJ1 cKO mice
293 (Figure 6E). In both SJ1 cKOTH and SJ1 cKO^{DAT} mice, EGFP expression was observed in TH-
294 positive DA soma within the SNc and VTA, as well as in their DA fibers projecting to the
295 striatum (Figures 6F and 6G). Similar to AAV5-flex-tdTomato, only a subset of local TH-
296 positive iTHINs expressed EGFP in the SJ1 cKO striatum but not B6 control (Figure 6G and
297 6H). To confirm the selectivity of this connection, we repeated the AAV9-TH-EGFP midbrain
298 labeling in Ai9;SJ1 cKOTH mice, in which all striatal THINs expressed tdT (Figure S9C). As
299 shown in Figure S9D, EGFP expression was exclusively detected in tdT/TH-positive double
300 positive iTHINs but absent in tdT-positive/TH-negative original WT THINs, reinforcing the
301 notion of selective connectivity between DA neurons and iTHINs.

302 As a third approach, we injected AAV-hSyn-mCherry into the ventral midbrain of SJ1 cKO
303 mouse models (Figure 6I). As expected, the pan-neuronal hSyn promoter drove mCherry
304 expression in different neurons near the injection site, including a subset of TH-positive DA
305 neurons in the midbrain of both SJ1 cKO^{TH} and SJ1 cKO^{DAT} (Figure 6J). Interestingly, in the
306 striatum of SJ1 cKO—but not WT mice, we observed mCherry-expressing neurons that were
307 exclusively iTHINs (anti-TH positive), suggesting specific connectivity and material transfer
308 (Figures 6K and 6L). In contrast, direct injection of AAV-hSyn-mCherry into WT striatum
309 resulted in random labeling of various local neurons, including Darpp32-positive MSNs and
310 other neuronal types (Figures S9E and S9F). This result further ruled out the possibility of
311 non-specific AAV leakage from dystrophic DA terminals in SJ1 cKO striatum.

312 Together, these three independent approaches provide compelling evidence that DA neurons
313 and iTHINs establish a selective and novel connection following SJ1 loss in the DA system.

314 **Upregulation of DA markers in iTHINs distinguishes SJ1 cKO from acute DA lesion**
315 **mouse models**

316 Previous studies using neurotoxin-induced PD rodent and non-human primate models have
317 shown the increase of THINs in the striatum following DA depletion[40-43]. To further characterize
318 the iTHINs observed in our genetic SJ1 cKO models, we directly compared them with two
319 acute DA lesion models: (1) the 6-OHDA model and (2) a caspase-3 (Casp3)-mediated
320 ablation model. In the 6-OHDA paradigm, B6 mice received a unilateral injection of the
321 neurotoxin into the midbrain, and brains were collected for IHC analysis two weeks post-
322 injection (Figure 7A). For the Casp3 lesion model, a Cre-dependent AAV-taCasp3-TEVp was
323 unilaterally injected into the midbrain of DAT-Cre mice, and brain tissue analyzed one-month
324 post-injection (Figure 7C). In both models, we observed clear evidence of DA neuron
325 degeneration in the midbrain and a near-complete loss of DA projections in the striatum
326 (Figures 7B and 7D). Following the depletion of DA fibers, a population of local TH-positive
327 neurons emerged in the striatum (Figure 7E), consistent with previously reported "THINs"[33] .
328 However, compared to the striatum of SJ1 cKO mice, 1) the TH protein expression level is
329 much weaker in these neurons (Figures 7E and 7F); 2) they did not express other DA-related
330 markers, including AADC and ALDH1A1 (Figure 7G and 7H); 3) they did not exhibit
331 endogenous DAT promoter activity (under the Ai9;DAT-Cre background, Figure S10A),
332 indicating that iTHINs in SJ1 DA cKO striatum acquire more DA-like features. In Table S1, we
333 summarized the differences between iTHINs in SJ1 DA cKO mice and WT THINs from these
334 two neurotoxin models.

335 In summary, various labeling strategies revealed that about 30% of the original WT THINs
336 were specifically induced to express DA-like features (TH/AADC protein and DAT promoter
337 activity) following DA-specific SJ1 cKO. In these iTHINs, a subset in the dorsal striatum also
338 expressed the A9 DA-specific marker ALDH1A1, matching their nigrostriatal DA input from the
339 midbrain. Furthermore, iTHINs appear to form new and specific connections with dystrophic
340 DA terminals, further supporting a role in adaptive compensation for DA deficiency (Figure
341 S10B).

342 **Acute SJ1 KO in Adulthood Triggers Similar DA Terminal Pathology with limited**
343 **Developmental Compensation from iTHINs**

344 As described above, iTHINs in genetic SJ1 cKO mice begin to appear at 2-3 weeks of age,
345 peaking at 2-3 months, suggesting that this is an adaptation during early development stage.
346 To bypass this developmental adaption, we generated acute SJ1 KO mice in DA neurons by
347 unilaterally injecting AAV-TH-Cre virus into the ventral midbrain of adult (2-month) or aged
348 (12-month) SJ1 flx/flx mice (Figure 8A). To assess the potential non-specific toxic effect of
349 AAV-Cre expression in DA neurons[44,45], we performed parallel injections in WT mice and found
350 no loss of DA somata or fibers (Figures S11A and S11B).

351 Following AAV injection, we confirmed successful acute KO of SJ1 by examining brain tissue
352 sections 3-4 months post injection, observing efficient depletion of SJ1 in most TH-positive
353 DA neurons on the ipsilateral midbrain (Figure 8B). Immunostaining results revealed
354 numerous TH/DAT-positive clusters throughout the striatum, resembling the DA terminal
355 pathology observed in genetic SJ1 cKO mice (Figures 8C and 8D). This confirms the synaptic
356 defects across the entire DA population projecting to the striatum due to the complete loss of
357 SJ1. Importantly, even though the number and density of DA terminal clusters in the striatum
358 were comparable to those observed in genetic SJ1 cKO mice, very few TH-positive iTHINs
359 were detected---about 10% of the number observed in genetic SJ1 cKO mice (Figures 8E and
360 8F). While the DA pathology resulting from SJ1 acute KO was comparable in adult and aged
361 mice, our findings suggest that the secondary compensatory response from iTHINs is primarily
362 induced during early development to compensate for DA terminal defects. Future longitudinal
363 studies are needed to determine whether acute SJ1 loss leads to progressive DA
364 neurodegeneration and motor deficits via axonal die-back.

365 **Discussion**

366 In this study, we examined the consequences of SJ1 loss in DA neurons using newly
367 generated DA-specific SJ1 cKO mice. We identified two major cellular outcomes: (1) a primary

368 defect marked by severe dystrophy of DA terminals, with accumulation of DA markers and
369 excess membranes in both dorsal and ventral striatum; and (2) a localized compensatory
370 response involving a robust increase in DA-like striatal TH-positive interneurons (iTHINs) that
371 communicate with DA terminals. Comparative analysis with acute adult SJ1 deletion and other
372 lesion models indicates that this iTHINs induction is specific to early developmental loss of
373 SJ1. This adaptive striatal plasticity may serve as an early neuroprotective mechanism to
374 maintain DA homeostasis or delay terminal degeneration, offering a potential therapeutic
375 strategy to preserve DA function in PD.

376 **Cell-Autonomous, Clathrin-Independent Role of SJ1 in the Neuromodulatory System**

377 SJ1 has been extensively studied in excitatory and inhibitory synapses, where it plays a key
378 role in clathrin uncoating during clathrin-mediated SV endocytosis and recycling. Constitutive
379 whole-body SJ1 KO mice die postnatally with severe epilepsy, suggesting imbalanced
380 excitatory/inhibitory transmission during development[16]. While DA-specific SJ1 cKO mice
381 survive to adulthood without seizures, our findings show that DA terminals from both the SNc
382 and VTA undergo significant dystrophic changes, indicating a cell-autonomous role for SJ1 in
383 regulating DA synaptic function. Surprisingly, no accumulation of endocytic proteins involved
384 in CME or CCVs were detected in these dystrophic terminals. As neuromodulators, DA
385 neurons release transmitters via "volume transmission," a slower process that does not rely
386 on precise synaptic contact sites[46]. This contrasts with the fast "synaptic transmission" seen
387 in excitatory and inhibitory synapses, which primarily recycle SVs through CME. Given these
388 differences, it is plausible that DA synapses utilize alternative mechanisms for SV recycling,
389 such as bulk endocytosis [47].

390 In addition to DA, another neuromodulator norepinephrine neurons are also vulnerable in PD,
391 likely due to shared features such as pace-making firing, extensive axonal arborization, and
392 accumulation of cytosolic oxidized catecholamines. Future studies using our SJ1 conditional
393 KO model could determine whether SJ1 similarly regulates SV recycling in norepinephrine
394 neurons and how its dysfunction contributes to their selective degeneration in PD.

395 **Gene Dosage-Dependent SJ1 Loss Correlates with the Severity of DA pathology**

396 There is a clear genotype-phenotype correlation in SJ1-linked PD cases, which is mirrored in
397 mouse models carrying different SJ1 mutations. DA pathology in these models also reflects
398 SJ1 gene dosage. The SJ1-KI^{RQ} model shows selective degeneration of nigrostriatal terminals,
399 while the SJ1 cKO model exhibits more widespread DA terminal dystrophy. This indicates that
400 both A9 and A10 DA neurons are susceptible to impaired SJ1-mediated SV recycling, with A9

401 SNc neurons being particularly vulnerable, even with partial SJ1 loss. A similar synergistic
402 effect is seen in the Auxilin KO/SJ1-KI^{RQ} double mutant, which displays more severe DA
403 terminal pathology than either single mutant[21]. More recently, SJ1 haploinsufficiency has been
404 linked to abnormal mesolimbic signaling and mild motivational deficits[48], suggesting a broader
405 role for SJ1 in VTA DA function that can be further explored using our SJ1 DA cKO mice.
406 Together, these findings highlight impaired SV recycling as a key driver of DA dysfunction,
407 with partial impairment leading to selective degeneration of SNc DA terminals as a hallmark
408 of PD pathogenesis.

409 **Synaptic Transmission Defects in DA Terminals Are Insufficient to Trigger Motor**
410 **Dysfunction**

411 SJ1 DA-specific cKO mice do not exhibit obvious motor deficits, despite showing more severe
412 terminal pathology and DA deficiency than SJ1-KI^{RQ} mice. This surprising finding suggests
413 several possibilities: (1) motor symptoms in SJ1-KI^{RQ} mice may arise from combined SJ1
414 dysfunction across multiple brain regions, not just DA neurons; (2) the dystrophic DA terminal
415 changes observed in SJ1 mutant mice may represent a prodromal phase of PD that does not
416 progress to full clinical manifestations within the mouse lifespan; and (3) local compensatory
417 mechanisms within the striatum may preserve basic motor function despite significant synaptic
418 dysfunction.

419 Our findings are consistent with recent studies using DA-specific cKO mouse models of two
420 important synaptic transmission proteins: the Ca^{2+} sensor Syt1 and the release site organizer
421 RIM1/2[49,50]. In both cKO models, although activity- or action potential-induced phasic DA
422 release is significantly abolished, the mice do not exhibit obvious motor defects[49,50].
423 Furthermore, early compensatory changes, such as receptor adaptation and enhanced DA
424 synthesis, packaging, and innervation, have been observed in the striatum of Syt1 DA-cKO
425 mice[49]. These results suggest that DA-dependent motor functions can be sustained by basal
426 extracellular DA levels and striatal compensatory plasticity.

427 Taken together, the converging results from three DA-specific cKO models with impaired
428 synaptic transmission support the idea that motor symptoms of PD only emerge after
429 extensive DA denervation. These models may therefore capture key aspects of the pre-
430 symptomatic or early compensatory stages of PD.

431 **Adaptive Compensation of iTHINs in SJ1 DA cKO Striatum**

432 *DA-like Features of iTHINs*

433 A prominent adaptive change in SJ1 DA cKO mice is a robust increase in iTHINs, accounting
434 for ~30% of the original total THINs population in the striatum. A much milder induction of
435 iTHINs was also observed in SJ1-KI^{RQ} and Auxilin KO/SJ1-KI^{RQ} double mutants, suggesting
436 that this response is specific to endocytic defects and modulated by gene dosage[21].

437 Neurotoxin-induced PD models (6-OHDA, MPTP) in rodents and non-human primates have
438 shown increased THINs in the striatum following DA depletion, suggesting a potential
439 compensatory or protective role[40-43]. However, it remains debatable whether these THINs
440 qualify as bona fide DA neurons capable of expressing key DA markers (e.g., AADC, DAT)
441 and producing/releasing DA[33,43,51].

442 In our study, when compared with acute 6-OHDA and Casp3 lesion models, iTHINs in SJ1
443 cKO mice displayed distinct DA-like features: strong co-expression of TH and AADC,
444 activation of the DAT gene promoter, and expression of the SNc DA neuron marker ALDH1A1
445 in a subset of dorsal striatal iTHINs. While SV-related markers like vMAT2 were not detected,
446 it's worth nothing that non-vesicle mediated somato-dendritic DA release in the midbrain has
447 been proposed previously[52]. Future biochemical and physiological studies are needed to
448 determine iTHINs capacity for DA production and release. Alternatively, iTHINs may retain
449 their GABAergic interneuron identity and contribute to striatal homeostasis by modulating local
450 circuitry[33].

451 *Crosstalk Between iTHINs and Dystrophic DA Terminals in SJ1 cKO Striatum*

452 Our observations further support long-distance communication between DA neurons and
453 iTHINs. First, a subset of iTHINs expressing A9 SNc DA marker ALDH1A1, are enriched in
454 the dorsal striatum, the primary target of ALDH1A1-positive DA fibers. This indicates a region-
455 specific and circuit-dependent compensatory response to DA terminal degeneration. Second,
456 AAV-based tracing from SJ1 KO DA neurons leads to selective co-labeling of striatal iTHINs,
457 suggesting material transfer or spreading from degenerating DA terminals to iTHINs. The
458 underlying mechanisms such as through newly formed synapses or non-synaptic mechanisms
459 such as exosomes or tunneling nanotubes should be explored in future studies[53,54].

460 What signal do striatal THINs detect to trigger their conversion? While extracellular DA levels
461 were previously shown to negatively regulate THINs number[55], acute DA lesion models with
462 severe DA depletion do not induce iTHINs. This indicates that other factors—likely released
463 from DA fibers—are required to initiate and sustain DA-like features in iTHINs. Notably, acute
464 SJ1 loss in adult or aged DA neurons significantly reduced the number of iTHINs, suggesting

465 this signal diminishes with age. Identifying this signal could open new therapeutic avenues for
466 circuit-level compensation in PD.

467 Furthermore, prior studies suggest THINs form connections with other striatal neurons[27,34],
468 raising the possibility that iTHINs may also engage in local crosstalk—an area that can be
469 further explored using single-nucleus RNA sequencing and spatial transcriptomics.

470 **Methods and Materials**

471 **Animals**

472 Mice were housed in SPF rooms with a 12-hour light/dark cycle. All experiments involving
473 animals were conducted according to the protocol approved by SingHealth Institutional Animal
474 Care and Use Committee (IACUC).

475 SJ1-KI^{RQ} mouse line was generated as described before and a gift from Prof Pietro De Camili
476 (Yale University)[20]. SJ1 flx/flx (C57BL/6J-Synj1^{em1cyagen}; S-CKO-00357, Cyagen) was
477 generated by inserting loxP sites flanking exon 4 of Synj1 using CRISPR/Cas9. These mice
478 were crossed with DAT-IRES-Cre (C001024, Cyagen) and TH-IRES-Cre knock in line
479 (generated from Prof Luis de Lecea Lab, Standford University; kindly provided by Dr Sarah
480 Luo, IMCB-A*STAR) to obtain double heterozygous, +/DAT-Cre;SJ1 +/flx and +/TH-Cre;SJ1
481 +/flx mice, respectively. To create DA-specific SJ1 conditional KO mice, double heterozygous
482 mice were crossed with homozygous SJ1 flx/flx, obtaining +/DAT-Cre;SJ1 flx/flx and +/TH-Cre;
483 SJ1 flx/fox mice, referred to as SJ1 cKO^{DAT} and SJ1 cKOTH, respectively. Appropriate littermate
484 or age-matched controls (SJ1 flx/flx or +/DAT-Cre;SJ1 +/flx or +/TH-Cre;SJ1 +/flx) were used
485 in all experiments. All mice used in the experiments with Cre-dependant promoter were
486 heterozygous, simply referred as DAT-Cre and TH-Cre in the manuscript.

487 Ai9 mice (B6.Cg-Gt(ROSA)26Sortm9(CAG-tdTomato)Hze/J; RRID:IMSR_JAX:007909) were
488 kindly provided by Prof Enrico Petretto (Duke-NUS) for specific labeling following Cre-
489 mediated recombination. Homozygous Ai9 mice were first crossed with homozygous SJ1
490 flx/flx to obtain double heterozygous, +/Ai9;SJ1 +/flx mice. Subsequent models involving Ai9
491 were all heterozygous Ai9, hence simply referred as Ai9 in the manuscript. Ai9;SJ1 +/flx mice
492 were then crossed with SJ1 cKO^{DAT} and SJ1 cKOTH to obtain Ai9;SJ1 cKO^{DAT} and Ai9;SJ1
493 cKOTH, respectively. Appropriate littermate or age-matched controls were used in all
494 experiments.

495 For SJ1 acute KO mice model, SJ1 flx/flx mice were employed. Briefly, mice were stereotactic
496 injected AAV.rTH.PI.Cre.SV40 (1ul) (Addgene-#107788) unilaterally in right midbrain (AP 3.3

497 mm, ML 1.2 mm, DV 4.3 mm) after anesthetized by isoflurane (5% induction, 2% maintenance
498 at 0.5-0.8 L/min oxygen or air flow). After 3 to 4 month of injection, mice brain tissues were
499 obtained for IHC.

500 For 6-hydroxydopamine (6-OHDA; H4381, Sigma-Aldrich) lesion model, B6 mice (C57BL/6J;
501 RRID:IMSR_JAX:000664**)** were treated with desipramine (D3900, Sigma-Aldrich; i.p. 25
502 mg/kg) 30 min prior to 6-OHDA infusions to prevent noradrenergic neurons. 6-OHDA (2.88 ug,
503 dissolved in 0.2% ascorbate/saline solution) was unilaterally pressure injected into the right
504 midbrain (AP 3.3 mm, ML 1.2 mm, DV 4.3 mm). Mice brain tissues were harvested for IHC
505 after 2 weeks of 6-OHDA injection.

506 For Casp3 ablation model, Cre-dependent virus, pAAV-flex-taCasp3-TEVp (1ul) (Addgene-
507 #45580) were unilaterally injected in Cre heterozygous mice right midbrain (AP 3.3 mm, ML
508 1.2 mm, DV 4.3 mm) after anesthetizing. Mice brain tissues were harvested for IHC after one
509 month of virus injection.

510

511 **AAV Labelling Surgery**

512 Animals were anesthetized using isoflurane (5% induction, 2% maintenance at 0 .5-0.8 L/min
513 oxygen or air flow) and secured in a stereotaxic apparatus. For virus injection, pAAV-FLEX-
514 tdTomato (1ul) (Addgene-#28306), rAAV-mTH-EGFP (BrainCase-#BC-0319) (0.5ul) or pAAV-
515 hSyn-mCherry (Addgene-#114472) (1ul) was infused into the midbrain (targeting the VTA and
516 SNc) and the striatum. The coordinates for the midbrain were AP 3.3 mm, ML 1.2 mm, DV 4.3
517 mm. For striatal infusion, the coordinates were AP -0.3 mm, ML -2.0 mm, DV -2.5 and -4.0
518 mm.

519 Infusions were conducted using a Hamilton syringe (Hamilton-Syringe, NEUROS, 7002, 2UL.
520 The infusion rate for all surgery was 100nl/min, unless stated otherwise. Syringe was left in
521 place for an additional 10 min before withdrawal to prevent retrograde mass flow. All injection
522 procedures were performed on a heating pad (37°C) to maintain body temperature. Following
523 surgery, mice recovered in another clean cage on a heating pad until they were awake.

524

525 **Antibodies**

526 The antibodies used in this study were obtained from commercial sources as stated: mouse
527 anti-α-synuclein (610786, RRID: AB_2748880), mouse anti-AP2 (611350, RRID: AB_398872)
528 and mouse anti-Dynamin (610245, RRID: AB_397640) from BD Biosciences; goat anti-ChAT

529 (AB144P, RRID: AB_2079751), mouse anti-clathrin light chain (AB9884, RRID: AB_992745),
530 rat anti-DAT (MAB369, RRID: AB_2190413), mouse anti-SV2C (MABN367, RRID:
531 AB_2905667) and rabbit anti-TH (AB152, RRID: AB_390204) from Merck Millipore; mouse
532 anti-β-actin (sc-47778, RRID: AB_2714189) and mouse anti-BIN1 99D (sc-13575,
533 RRID:AB_626753) from Santa Cruz Biotechnology; rabbit anti-ALDH1A1 (HPA002123, RRID:
534 AB_1844722), rabbit anti-GFAP (ZRB2383, RRID: AB_2905668) and rabbit anti-SJ1
535 (HPA011916, RRID: AB_1857692) from Sigma-Aldrich; rabbit anti-Endophilin 1 (159002, RID:
536 AB_887757), mouse-anti Calretinin (214111, RRID: AB_2619904), mouse anti-TH (213211,
537 RRID: AB_2636901), rabbit anti-Amphiphysin 1 (120002, RRID: AB_887690), rabbit anti-
538 AADC (369003, RRID: AB_2620131), guinea pig-anti Calbindin D28k (214005, RRID:
539 AB_2619902), mouse anti-Parvalbumin (195011, RRID: AB_2619883) and rabbit anti-D2R
540 (376 203, RRID: AB_2636918) from Synaptic Systems; rabbit anti-VMAT2 (MSFR106400,
541 RRID: AB_2571857) from Nittobo Medical; rabbit anti-DARPP-32 (2306, RRID: AB_823479)
542 and rabbit anti-Neuropeptide Y (11976, RRID: AB_2716286) from Cell Signaling Technology;
543 rabbit anti-Iba1 (019-19741, RRID: AB_839504) from FUJIFILM Wako Pure Chemical
544 Corporation; goat anti-ALDH1A1 (AF5869_RRID: AB_2044597) from R&D Systems; rabbit
545 anti-alpha synuclein phospho S129 (EP1536Y, RRID:AB_765074) from abcam; mouse anti-
546 GAPDH (60004-1, RRID: AB_2107436) and rabbit anti-GAPDH (10494-1-AP, RRID:
547 AB_2263076) from Proteintech.

548 Secondary antibodies used were all purchased from commercial sources as stated: donkey
549 anti-mouse IgG (H + L) Alexa Fluor Plus 488 (A32766, RRID: AB_2762823), donkey anti-
550 mouse IgG (H + L) Alexa Fluor 594 (A21203, RRID: AB_2535789), donkey anti-mouse IgG
551 (H + L) Alexa Fluor Plus 647 (A32787, RRID: AB_2762830), donkey anti-rabbit IgG (H + L)
552 Alexa Fluor Plus 488 (A32790, RRID: AB_2762833), donkey anti-rabbit IgG (H + L) Alexa Fluor
553 Plus 594 (A32754, RRID: AB_2762827), donkey anti-rabbit IgG (H + L) Alexa Fluor 647
554 (A32795, RRID: AB_2762835), donkey anti-rat IgG (H + L) Alexa Fluor Plus 488 (A48269,
555 RRID: AB_2893137), donkey anti-rat IgG (H + L) Alexa Fluor 594 (A21209, RRID:
556 AB_2535795), donkey anti-goat IgG (H + L) Alexa Fluor 488 (A11055, RRID: AB_2534102),
557 donkey anti-goat IgG (H + L) Alexa Fluor 594 (A32758, RRID: AB_2762828), goat anti-guinea
558 pig IgG (H + L) Alexa Fluor 488 (A11073, RRID: AB_2534117) and goat anti-guinea pig IgG
559 (H + L) Alexa Fluor 647 (A21450, RRID: AB_2535867) from Life Technologies; goat anti-
560 mouse IgG light chain HRP (AP200P, RRID:AB_805324) and mouse anti-rabbit IgG light chain
561 HRP (MAB201P, RRID:AB_827270) from Merck; IRDye 800CW donkey anti-rabbit IgG (926-
562 32213, RRID: AB_621848), IRDye 800CW donkey anti-mouse IgG (926-32212, RRID:
563 AB_621847), IRDye 680RD donkey anti-mouse IgG (926-68072, RRID: AB_10953628) and
564 IRDye 800CW goat anti-rat (926-32219, RRID: AB_1850025) from LI-COR Biosciences.

565

566 **Brain Histology and Immunofluorescence**

567 Mice were anesthetized with a Ketamin/Xylazine anesthetic cocktail injection, perfused
568 transcardially with ice-cold 4% paraformaldehyde in 1 X phosphate-buffered saline (PBS) and
569 the brains were kept in the same fixative overnight at 4°C. On the next day, brains were
570 transferred to 30% sucrose in 1 X PBS and kept overnight at 4°C on top of a roller. Brains
571 were then embedded in OCT (Tissue-Tek) and freeze in liquid nitrogen-cooled 2-methylbutane
572 (Isopentane). Coronal or sagittal sections of 20 µm thickness were cut with a cryostat. The
573 sections were either mounted on adhesive slide, SuperFrost® Plus (VWR) or collected as
574 floating sections in 1 X PBS in a 24-well plate. Sections were then blocked in 5% BSA and
575 0.1% Triton X-100 in 1 X PBS for 1 hour at room temperature. After blocking, sections were
576 incubated with primary antibodies and kept overnight at 4°C. Subsequently, sections were
577 washed 3 times for 10 min with 0.1% Triton X-100 in 1 X PBS, then incubated with Alexa-
578 conjugated secondary antibodies for 1 hour at room temperature. Finally, the sections were
579 mounted with Fluoromount-G (Invitrogen) and sealed with nail polish. The floating sections
580 were mounted onto slides after all the staining procedures. Images were acquired with Andor
581 BC43 (Oxford Instruments) with 10x, 20x and 40x oil objective or a spinning disk system
582 (Gataca Systems) based on an inverted microscope (Nikon Ti2-E; Nikon) equipped with a
583 confocal spinning head (CSU-W, Yokogawa) and a Plan-Apo 20x and 40x oil objective.

584 For stereological analysis of TH-positive DA neurons in the midbrain, 30 µm coronal section
585 were collected incubated with 0.1% H2O2 for 5 min to quench endogenous peroxidase activity
586 and subsequently incubated with buffer containing 5% BSA, and 0.1% Triton X-100 in 1X PBS
587 for 1 hour at room temperature. Next, sections were incubated overnight at 4°C with anti-TH
588 primary antibody (1:1000). The sections were then washed with 1X PBS three times for 10
589 min and incubated with a biotinylated anti-rabbit secondary antibody (Vector Laboratories,
590 USA) for 1 hour at room temperature, later followed by incubation with Avidin/Biotin complex
591 (ABC) reagent (Vector Laboratories, USA) at room temperature. Finally, immunoreactivity was
592 revealed by incubation with diaminobenzidine (DAB). Stereological analysis was performed
593 using the optical fractionator probe in the Stereo Investigator (MBF Bioscience) software. A
594 total of 7-9 coronal sections of every fourth sections were collected across the midbrain and
595 used for counting. The SN and VTA regions were outlined based on the Allen mouse brain
596 atlas and counting was performed using 63x oil lens. The parameters used were guard zone
597 of 2 µm, dissector height of 13 µm and counting frame of 200 µm x 200 µm.
598

599 **Electron Microscopy**

600 2 months old mouse was anesthetized and fixed by transcardial perfusion with 4%
601 paraformaldehyde and 0.125% glutaraldehyde (EMS, Hatfield, PA) in 0.1 M PB buffer. Brain
602 was removed and dissected in small pieces ($1 \times 1 \times 1\ mm^3$) and further incubated in 2.5%
603 glutaraldehyde in 0.1 M PB buffer at 4 °C overnight. The samples were then washed for 5 mins
604 in 1 X PBS for three times. The samples were post-fixed with 1% osmium tetroxide for 1 hour
605 and washed with distilled water. They are then dehydrated through an ethanol series (25%,
606 50%, 75%, 95% and 100%) and absolute acetone, before infiltrating with araldite
607 resin/acetone mixtures. On the next day, samples were further infiltrated in pure resin at 40°C
608 to 50°C, then embedded in resin and polymerised at 60°C for 24 hours. The embedded sample
609 was sectioned into 100nm slices with a Leica UC6 ultramicrotome and stained with lead citrate.
610 Images were captured with JEOL JEM-1400Flash TEM, operating at 100kV.

611

612 **Motor Behavioral Tests**

613 SJ1 cKO^{DAT} and mice between 2-8 months old were used for balance beam and rotarod tests.
614 The mice were divided into two age groups: 2-3 months old (n= 13 for Ctrl, n=15 for SJ1
615 cKO^{DAT}) and 6-8 months old (n=9 for Ctrl and n=10 for SJ1 cKO^{DAT}). Both males and females
616 were used for the behavioral assays. Both tests were conducted during the light period. The
617 mice were allowed to be acclimatized to the test for at least 30 min before each test.

618 *Balance Beam Test*

619 A narrow beam (10 mm width) was suspended 15 cm above a soft padding. Mice were placed
620 on end of the beam and during their trip towards the other end, the number of missteps (paw
621 slips) was recorded. The test was conducted thrice for each mouse and the average number
622 of missteps was calculated.

623 *Rotarod Test*

624 Mice were placed on a rod which is rotating at 4 rpm with an acceleration to 40 rpm within 6
625 min. The duration of the mice staying on the rod is measured three times at 10 min intervals
626 and the average 'latency to fall' was determined for each mouse.

627 *Open Field Test*

628 Mice were placed in a chamber measured 40 cm (length) x 40 cm (width) x 30 cm (height)
629 and recorded for 15-minute. Recorded videos were analyzed with TopScan video tracking
630 software. The mice path tracking and time spent in the defined area were analyzed. The mice
631 used for two age groups: 2-3 months old (n= 12 for Ctrl, n= 14 for SJ1 cKO^{DAT}) and 6-8 months
632 old (n= 6 for Ctrl and n= 7 for SJ1 cKO^{DAT}).

633

634 **HPLC**

635 Striatum tissues dissected from mice brain were homogenized in 0.5 N perchloric acid with
636 100 µM of deferoxamine mesylate and 100 µM of glutathione. The homogenized samples
637 were further sonicated, centrifuged and the supernatants were filtered using 0.1 µm PVDF
638 centrifugal filters before collecting the filtrates for HPLC analysis. A reversed-phase UltiMate
639 3000 HPLC system (Thermo Fisher Scientific) with an electrochemical detector and a
640 reversed-phase column (Vydac Denali, C18, 4.6 x 250 mm, 5 µm particle size, 120 Å pore size)
641 were used to run the samples. The HPLC run was performed at a flow rate of 0.5 ml per minute
642 with a mobile phase containing 1.3% sodium acetate, 0.01% EDTA (pH8.0), 0.5% sodium 1-
643 heptanesulfonate, 7% acetonitrile (v/v) and 2% methanol (v/v), adjusted to pH 4.0 with acetic
644 acid. All buffers used for HPLC analysis were double filtered through 0.2 µM nylon membranes.
645 Dopamine, DOPAC and HVA levels in the samples was identified by retention time of their
646 respective standard and quantified by measuring the area under the peak using the software
647 ChromeleonTM 7.2 Chromatography Data System (Thermo Fisher Scientific). The areas
648 under the peaks were normalized to their respective tissue weight.

649

650 **Immunoblotting**

651 Striatum tissues were homogenized in buffer containing 20 mM Tris-HCl (pH 7.4), 150 mM
652 NaCl, 2 mM EDTA and cOmpleteTM EDTA-free Protease Inhibitor Cocktail (Roche, USA). The
653 homogenized samples were centrifuged at 700 g for 10 min to obtain the post-nuclear
654 supernatant (PNS). Protein concentration was determined by the Pierce BCA Protein Assay
655 Kit. SDS-PAGE and western blotting were performed by standard procedures. The
656 membranes were blotted with primary antibodies and then IRDye® Secondary Antibodies (LI-
657 COR, USA) or HRP light chain secondary antibodies. The protein bands were detected using
658 Odyssey ® CLx imaging system or Bio-Rad ChemiDoc Touch Imaging System, and its
659 intensity was quantified via Image Studio. A minimum of three independent sets of samples
660 were used for quantification.

661

662 **Quantification of DAT Immunoreactivity Clusters and TH+ Striatal Interneurons**

663 The quantification of DAT-positive clustering in striatum was conducted using Fiji software
664 (Version ImageJ 2.160/1.54p/Java 1.8.0_322 (64-bit), RRID: SCR_002285). For each mouse,
665 5 random sampling sites with a size of 300 µm x 300 µm were selected respectively for both

666 dorsal and ventral striatum. At least three mice from each genotype and each age group were
667 collected for this purpose. The threshold setting for the clusters was set to quantify puncta
668 bigger than 5 μm^2 to ensure normal positive axonal terminals were not counted in. The
669 average size of clusters and average number of clusters was counted automatically with Fiji
670 plugin "Analyse Particles" based on all five random sampling sites for each mouse.

671 Quantification of TH-positive and tdT-expressing cells was done using Fiji software with full
672 stitched half coronal section. Image acquisition involved tiling of the entire section with either
673 10x or 20x objective lens on Andor BC43. Cell Counter plugin in Fiji software was used to
674 count visible cell bodies across the striatum (outlined based on Allen mouse brain atlas). Cell
675 count from individual channels was used for percentage ratio quantification.

676 Quantification for TH-positive cells intensity was done using Fiji software. A consistent
677 threshold was applied across all images to isolate TH-positive signals. The 8-bit figure type
678 was used to measure the mean density of the TH signal. Background fluorescence was
679 determined from adjacent areas without specific staining. All measurements were performed
680 under identical settings to ensure consistency across experimental groups. For each mouse,
681 6 random TH-positive cells were selected from both dorsal and ventral striatum. At least three
682 mice from each condition were collected for this purpose.

683

684 **Statistical Analysis**

685 All statistical analysis was performed using GraphPad Prism (Ver 10.4.1, RRID: SCR_002798).
686 All graphs were plotted on GraphPad Prism. Data are presented as mean ± SEM unless
687 otherwise stated. Statistical significance was determined using the Student's unpaired *t* test
688 for the comparison of two independent groups or ANOVA with Tukey's Honest Significant
689 Difference post hoc test for multiple group comparisons. Data with *p*-values <0.05, <0.01,
690 <0.001, and <0.0001 are represented by asterisks *, **, ***, and ****.

691

692 **Acknowledgment**

693 We thank Prof Zhang Suchun's lab (Duke-NUS) and Asst Prof Jun Nishiyama's lab (Duke-
694 NUS) for providing some reagents for the experiments. We thank Prof Pietro De Camili (Yale
695 University), Prof Shirish Shenolikar (Duke University) and Prof Wang Hongyan (Duke-NUS)
696 for reading the manuscript and providing comments. We thank Dr Sarah Luo Xinwei (IMCB-
697 A*STAR) and Prof Enrico Petretto (Duke-NUS) for kindly providing TH-IRES-Cre mouse line
698 and Ai9 mouse line, respectively. We also thank Prof Pietro De Camili for gifting SJ1-KI^{RQ}

mouse line. We thank Asst Prof Wong Peiyan (Duke-NUS) from animal behaviour core for training. We thank Electron Microscopy Unit (NUS) for EM preparation and imaging. Select portions of this manuscript were edited for clarity and grammar using the ChatGPT language model (OpenAI). Scientific content and interpretations were solely formulated by the authors. This research was supported in part by grant from Ministry of Education Academic Research Fund (AcRF) Tier 2 Singapore (MOE-T2EP30122-0009) and Tier 1 (FY2024-MOET1-0001).

Declaration of interest

The authors declare no competing interests.

Author Contributions

B.M., Y.L., M.L., Z.L. and M.C. designed the experiments. Y.L., M.L. and Z.L. performed sample preparations, histology experiments and microscopy imaging. Y.L. and X.C performed HPLC and analysis. Y.L. preformed western blotting and analysis. Y.L. and M.C. performed sample preparations for EM. B.M., Y.L., M.L. and X.C. performed behavioural experiments and analysis. B.M., M.L. and Z.L. performed stereotaxic injections. Y.L. and M.L. performed quantification and statistical analysis. M.L. and X.C. performed mice genotyping. B.M., Y.L., M.L., Z.L. and M.C. wrote the paper. All authors read and approved the final manuscript.

Availability of data and materials

The datasets generated and/or analyzed in this study are available from the corresponding author Mian Cao on request.

722 **Figure Legends**

723 **Figure 1. SJ1 conditional KO (SJ1 cKO^{DAT}) in DA neurons exhibit dystrophic DA axon**
724 **terminals in the striatum**

725 (A) Generation of SJ1 cKO^{DAT} mice by crossing SJ1 flx/flx mice with DAT-IRES-Cre line to
726 create DA-specific SJ1 conditional KO mice (DAT-Cre;SJ1 flx/flx), hereafter referred to as SJ1
727 cKO^{DAT}. Appropriate littermate control (SJ1 flx/flx or DATCre;SJ1+/flx) were used in all
728 experiments.

729 (B) Double staining of TH and SJ1 to show SJ1 specifically KO in midbrain DA neurons. Green
730 arrows: TH-positive DA neurons; White arrows: TH-negative midbrain neurons. SJ1
731 expression in hippocampus shows that other regions were not affected. Scale bar: 20 μm.

732 (C) DAT staining of 2 months old Ctrl and SJ1 cKO^{DAT} shows clustering phenotype in dorsal
733 (DS) and ventral striatum (VS). Scale bar: 20 μm.

734 (D) Quantification for DAT clusters at 2-3 months and 6-8 months of age. The average number
735 of clusters is counted in five randomly selected, 300 × 300-μm regions of interest (ROIs). Data
736 are represented as mean ± SEM (**$p < 0.01$, and ***$p < 0.001$, and ****$p < 0.0001$ by one-way
737 ANOVA with post-hoc Tukey's test). n=3 mice per genotype.

738 (E) Double staining of DAT with TH, AADC, vMAT2 and SV2C showed colocalization in the
739 dorsal striatum (DS) of SJ1 cKO^{DAT} mice. Scale bar: 20 μm.

740 (F) Representative EM micrographs of nerve terminals from the ventral striatum (VS) of SJ1
741 cKO^{DAT}. Red arrows: "Whirl"-like multilayered membranes; Synaptic vesicles (SVs),
742 endosomes (endo), autophagosome (AP) and mitochondria (mt) were also labeled in the
743 images. Scale bar: 500 nm.

744

745 **Figure 2. DA deficiency in SJ1 cKO^{DAT} striatum with no apparent motor deficit**

746 (A) Representative blots for DA markers, including DAT, vMAT2, TH and AADC from 2-3
747 months old Ctrl and SJ1 cKO^{DAT} half brain striatal homogenates.

748 (B) Quantification of proteins level shown in (A). Significant reduction of DAT and vMAT2 in
749 SJ1 cKO^{DAT} after protein levels normalized to the level of actin. Data are represented as mean
750 ± SEM (**$p < 0.01$, and ***$p < 0.001$ with Student's unpaired t-test). n=3-5 mice per genotype.

751 (C), (D) HPLC analysis of SJ1 cKO^{DAT} mice showed an average of 50% reduction in striatal
752 DA levels for (C) 2-3 months old and (D) 6-8 months old. Data are represented as mean ± SEM

753 (*p < 0.05, **p < 0.01 by one-way ANOVA with Student's unpaired t-test). n=5 for Ctrl and 2-
754 3M SJ1 cKO^{DAT}; n=6 for Ctrl and 6-8M SJ1 cKO^{DAT}.

755 (E) Performance of SJ1 cKO^{DAT} mice in open field test. No significant difference in locomotor
756 activity at 2-3 months old. Significant p-value for total distance and center distance at 6-8
757 months old indicate reduced exploratory activity. Data are represented as mean ± SEM
758 (**p < 0.01 with Student's unpaired t-test). n numbers used for each age group of the Ctrl and
759 SJ1 cKO^{DAT} mice (2-3M: 12 and 14; 6-8M: 6 and 7).

760 (F) Representative tracing of Ctrl and SJ1 cKO^{DAT} mice at 2-3 months and 6-8 months old
761 recorded for 15 minutes. The center square box indicates the “center zone”.

762 (G) Performance of two age groups of SJ1 cKO^{DAT} mice on the accelerated rotarod. Data are
763 represented as mean ± SEM. n numbers used for each age group of the Ctrl and SJ1 cKO^{DAT}
764 mice (2–3M: 13 and 15; 6–8 M: 9 and 10).

765 (H) Quantification for the number of missteps during the balance beam test for two age groups
766 of SJ1 cKO^{DAT} mice. Data are represented as mean ± SEM. n numbers used for each age
767 group of the Ctrl and SJ1 cKO^{DAT} mice (2–3M: 13 and 15; 6–8M: 9 and 10).

768

769 **Figure 3. Robust appearance of induced TH-positive interneurons (iTHINs) with DA-like**
770 **characteristics in the SJ1 cKO^{DAT} striatum**

771 (A) Numerous induced TH-positive interneurons (iTHINs) observed in the striatum of SJ1
772 cKO^{DAT} mice but not in Ctrl. Scale bar: 50 µm.

773 (B) Quantification of iTHINs in 2-3 months and 6-8 months age group. Number of iTHINs were
774 quantified on single coronal striatum section of one hemisphere. Data are represented as
775 mean ± SEM (**p < 0.01). n=3 mice per genotype.

776 (C) Representative image of iTHINs expressing AADC in the striatum of 2 months old SJ1
777 cKO^{DAT} mice compared to Ctrl. White arrows: iTHINs. Asterisk: clusters. Scale bar: 20 µm.

778 (D) Double staining of vMAT2 and TH shows vMAT2 is clustered with TH at DA terminals but
779 not expressed in iTHINs in 2 months old SJ1 cKO^{DAT} striatum. White arrows: iTHINs. Asterisk:
780 clusters. Scale bar: 20 µm.

781 (E) Double staining of DAT and TH shows DAT is clustered with TH at DA terminals but not
782 expressed in iTHINs in 2 months old SJ1 cKO^{DAT} striatum. White arrows: iTHINs. Asterisk:
783 clusters. Scale bar: 20 µm.

784 (F), (G) Double staining of ALDH1A1 and TH shows ALDH1A1 is detected in both dystrophic
785 DA terminals and iTHINs in SJ1 cKO^{DAT} (F) dorsal but not (G) ventral striatum. White arrows:
786 iTHINs. Asterisk: clusters. Scale bar: 50 μm.

787

788 **Figure 4. SJ1 conditional KO using TH-IRES-Cre (SJ1 cKOTH) phenocopies SJ1 cKO^{DAT}**
789 **pathological characteristics**

790 (A) Generation of SJ1 cKOTH mice by crossing SJ1 flx/flx mice with TH-IRES-Cre line to create
791 TH-specific SJ1 conditional KO mice (TH-Cre;SJ1 flx/flx), hereafter referred to as SJ1 cKOTH.
792 Appropriate littermate controls (SJ1 flx/flx or TH-Cre;SJ1 +/flx) were used in all experiments.

793 (B) Double staining of TH and SJ1 showed specific loss of SJ1 in DA neurons. SJ1 expression
794 in hippocampus shows that other regions were not affected. Scale bar: 20 μm.

795 (C) DAT staining of 2 months Ctrl and SJ1 cKOTH showed similar clustering phenotype in
796 dorsal and ventral striatum. Scale bar: 20 μm.

797 (D) Double staining of vMAT2 with SV2C showed co-aggregation in the striatum of SJ1 cKOTH
798 mice. Scale bar: 20 μm.

799 (E) Double staining of DAT and TH showed DAT is clustered with TH at DA terminals (asterisk),
800 but not expressed in iTHINs (white arrows) in the striatum of SJ1 cKOTH mice. Scale bar:
801 20 μm.

802 (F) Double staining of AADC and TH showed AADC is clustered with TH at DA terminals
803 (asterisk), and also co-expressed in iTHINs (white arrows). Scale bar: 20 μm.

804 (G), (H) Double staining of ALDH1A1 and TH shows ALDH1A1 is detected in both dystrophic
805 DA terminals (asterik) and iTHINs (white arrows) in SJ1 cKO^{DAT} dorsal (G) but not ventral (H)
806 striatum. Scale bar: 50 μm.

807

808 **Figure 5. iTHINs emerge from original WT THINs and induce DAT gene expression after**
809 **SJ1 loss**

810 (A) Simplified schematic showing the generation of Ai9-tdT labeled SJ1 cKOTH and SJ1 cKO^{DAT}
811 mice, referred to as Ai9;SJ1 cKOTH and Ai9;SJ1 cKO^{DAT}, respectively. Ai9-tdT reporter driven
812 by CAG promoter expresses DA-specific tdT signal after Cre-mediated recombination by
813 either TH- or DAT-IRES-Cre line.

814 (B) Representative images of tdT expression and immunostaining of TH in the midbrain DA
815 neurons of 2 months old Ai9;TH-Cre (Ctrl) and Ai9;SJ1 cKOTH. Scale bar: 100 μm.

816 (C) Representative images of tdT expression and immunostaining of TH in the striatum of 2
817 months old Ai9;TH-Cre (Ctrl) and Ai9;SJ1 cKOTH. Blue arrows: tdT expressing THINs driven
818 by TH-Cre recombination (negative for TH immunostaining). White arrows: iTHINs expressing
819 tdT signal (positive for TH immunostaining). Scale bar: 50 μm

820 (D) Percentage of TH-Cre driven tdT expressing neurons positive for TH immunostaining
821 shown in (C). In average, 34.11% of total tdT expressing neurons were positive for TH
822 immunostaining (iTHINs). The number of neurons was quantified on a single stitched coronal
823 striatum section for both tdT expressing neurons and tdT/TH-positive neurons. Data are
824 represented as mean ± SEM. n=3 mice per genotype.

825 (E) Representative images of tdT expression and TH immunostaining of DA neurons in the
826 midbrain of 2 months old Ai9;DAT-Cre (Ctrl) and Ai9;SJ1cKO^{DAT}. Scale bar: 100 μm.

827 (F) Representative images of tdT expression and immunostaining of TH and DAT in the
828 striatum of Ai9;DAT-Cre (Ctrl) and Ai9;SJ1cKO^{DAT}. tdT expressing striatal neurons were
829 positive for TH but not DAT immunostaining, indicating DAT gene promoter is activated in
830 iTHINs but DAT protein is undetected. White arrows: all tdT-expressing THINs driven by DAT-
831 Cre that were positive for TH immunostaining. Scale bar: 50 μm.

832 (G) Percentage of DAT-Cre driven tdT expressing neurons positive for TH immunostaining
833 shown in (F). Majority of tdT expressing neurons were iTHINs. The number of neurons was
834 quantified on a single stitched coronal striatum section for both tdT expressing neurons and
835 tdT/TH-positive neurons. Data are represented as mean ± SEM. n=3 mice per genotype.

836

837 **Figure 6. iTHINs establish specific and new connection with dystrophic DA fibers in SJ1**
838 **DA cKO striatum**

839 (A) Schematic showing experiment procedure and timeline. pAAV-FLEX-tdTomato (Cre-
840 dependent) was injected unilaterally into the ventral midbrain of SJ1 cKOTH, SJ1 cKO^{DAT} mice
841 and Cre mouse controls at 2-3 months old. The animal brains were collected 2 weeks post
842 injection for IHC.

843 (B) Representative images of TH immunostaining and tdT expression in the injected midbrain
844 DA neurons of both SJ1 cKOTH and SJ1 cKO^{DAT} mice. Scale bar: 100 μm.

845 (C) Representative images of TH immunostaining in the striatum. While tdT injection in TH-
846 Cre and DAT-Cre mice only labeled some DA fibers, tdT injection in SJ1 cKO^{TH} and SJ1
847 cKO^{DAT} labeled both DA fibers and several iTHINs. White arrows: iTHINs double positive for
848 tdT signal and TH immunostaining. Scale bar: 50 μm.

849 (D Percentage of tdT expressing neurons positive for anti-TH staining in both SJ1 cKO^{TH} and
850 SJ1 cKO^{DAT}. The number of neurons was quantified on a single stitched coronal striatal section
851 for both tdT and TH/tdT-positive neurons. Data are represented as mean ± SEM. n=3 mice per
852 genotype.

853 (E) Schematic showing experiment procedure and timeline. rAAV-mTH-EGFP was unilaterally
854 injected into the midbrain of B6, SJ1 cKO^{TH} and SJ1 cKO^{DAT} mice at 2-3 months old. The
855 animal brains were collected 2 weeks post injection for IHC.

856 (F) Representative images of TH immunostaining with EGFP expression in the injected
857 midbrain DA neurons of both SJ1 cKO^{TH} and SJ1 cKO^{DAT} mice. Scale bar: 100 μm.

858 (G) Representative images of TH immunostaining and EGFP expression in the striatum. No
859 EGFP expressing THINs observed in B6 striatum. Striatum of injected SJ1 cKO^{TH} and SJ1
860 cKO^{DAT} mice show EGFP specifically expressed in iTHINs. White arrows: iTHINs double
861 positive for EGFP and anti-TH staining. Scale bar: 50 μm.

862 (H) Percentage of EGFP expressing neurons positive for anti-TH staining in both SJ1 cKO^{TH}
863 and SJ1 cKO^{DAT}. The number of neurons was quantified on a single stitched coronal striatal
864 section for both EGFP neurons and TH/EGFP-positive neurons. Data are represented as
865 mean ± SEM. n=3 mice per genotype.

866 (I) Schematic showing experiment procedure and timeline. pAAV-hSyn-mCherry was injected
867 unilaterally in the midbrain of B6, SJ1 cKO^{TH} and SJ1 cKO^{DAT} mice at 2-3 months old. The
868 animal brains were collected 2 weeks post injection for IHC.

869 (J) Representative images of TH immunostaining and mCherry expression in the injected
870 midbrain DA neurons of both SJ1 cKO^{TH} and SJ1 cKO^{DAT} mice. Scale bar: 100 μm.

871 (K) Representative images of TH immunostaining and mCherry expression in the striatum of
872 injected mice. No mCherry labeled THINs in B6 striatum. Striatum of injected SJ1 cKO^{TH} and
873 SJ1 cKO^{DAT} show mCherry specifically expressed in iTHINs. White arrows: iTHINs double
874 positive for mCherry and anti-TH staining. Scale bar: 50 μm.

875 (L) Percentage of mCherry expressing neurons positive for anti-TH staining in both SJ1 cKO^{TH}
876 and SJ1 cKO^{DAT}. The number of neurons was quantified on a single stitched coronal striatal

877 section for both mCherry and TH/mCherry-positive neurons. Data are represented as
878 mean ± SEM. n=3 mice per genotype.

879

880 **Figure 7. THINs appearing in 6-OHDA and Casp3 lesion mice are distinct from iTHINs**
881 **observed in SJ1 cKO mice**

882 (A) Schematic showing the midbrain of 2-3 months old B6 mice unilaterally injected with 6-
883 OHDA and collected 2 weeks post injection for IHC.

884 (B) Representative coronal section shows the extent of 6-OHDA lesion in the striatum and
885 midbrain DA neurons of B6 mice. Scale bar: 500 μm.

886 (C) Schematic showing the midbrain of 2-3 months old DAT-Cre mice unilaterally injected with
887 pAAV-flex-taCasp3-TEVp (Cre-dependent) and collected 1 month post injection for IHC.

888 (D) Representative coronal section shows the extent of Casp3-mediated lesion in the striatum
889 and midbrain DA neurons of DAT-Cre mice. Scale bar: 500 μm.

890 (E) Representative images of TH-positive neurons (white arrows) observed in the striatum of
891 SJ1 cKO^{DAT} and lesioned hemisphere of 6-OHDA and Casp3 injected mice. Exposure time
892 and threshold were set the same for anti-TH imaging in all three conditions. Scale bar: 20 μm.

893 (F) The expression of anti-TH neurons observed in 6-OHDA and Casp3 lesioned models is
894 significantly lower than iTHINs observed in SJ1 cKO^{DAT} striatum. Data are represented as
895 mean ± SEM (****$p < 0.0001$). n=3 mice per genotype.

896 (G) Unlike iTHINs in SJ1 cKO^{DAT} mice, AADC is undetectable in either 6-OHDA or Casp3
897 lesioned striatum. Scale bar: 20 μm.

898 (H) Unlike iTHINs in SJ1 cKO^{DAT} mice, ALDH1A1 is undetectable in either 6-OHDA or Casp3
899 lesioned striatum. Scale bar: 20 μm.

900

901 **Figure 8. Acute SJ1 KO in DA neurons of adult and aged mice triggers similar DA**
902 **terminal pathology but fewer iTHINs**

903 **(**A) Schematic showing unilateral stereotaxic injection of AAV9-TH-Cre virus into the ventral
904 midbrain of 2 months (adult) or 12 months (aged) SJ1 flx/flx mice to obtain SJ1 acute KO in
905 DA neurons. Animal brains were collected 3-4 months post injection for IHC.

906 (B) TH and SJ1 immunostaining of the adult and aged SJ1 acute KO mice showed SJ1 specific
907 KO in the injected midbrains. Scale bar: 100 μm.

908 (C) DAT immunostaining of the adult and aged SJ1 acute KO mice shows similar clustering
909 phenotype in dorsal (DS) and ventral striatum (VS) as observed in SJ1 cKO^{DAT} mice. Scale
910 bar: 20 µm.

911 (D) No significant difference of the number of DAT clusters between SJ1 cKO^{DAT}, adult and
912 aged SJ1 acute KO. The average number of clusters is counted in five randomly selected,
913 300 × 300-µm regions of interest (ROIs). Data are represented as mean ± SEM. n = 3-4 mice
914 per genotype.

915 (E) Representative images of striatum show comparable TH/DAT-positive clusters but much
916 lesser iTHINs in the injected hemisphere of adult and aged SJ1 acute KO mice when
917 compared to SJ1 cKO^{DAT}. White arrows: iTHINs. Scale bar: 50 µm.

918 (F) Number of iTHINs in the adult and aged SJ1 acute KO is significantly lower than SJ1
919 cKO^{DAT} mice. Number of iTHINs was quantified in stitched coronal section of the injected
920 striatum. Data are represented as mean ± SEM (**$p < 0.01$). n=3-4 mice per genotype.

921

922

923 **Supplementary Figure Legends**

924 **Supplementary Figure 1. Further Characterization of DA system in SJ1 cKO^{DAT} mice**

925 **(**A) Generation strategy to obtain SJ1 cKO^{DAT} mouse model. Heterozygous DAT-IRES-Cre line
926 was crossed with homozygous SJ1 flx/flx to obtain double heterozygous DAT-Cre;SJ1 +/flx.
927 Double heterozygous were further crossed with each other to obtain SJ1 cKO^{DAT} and control
928 mice.

929 (B) Stereological analysis of TH-positive DA cell bodies in the SN and VTA region of Ctrl and
930 SJ1 cKO^{DAT} mice at 2-3 months and 6-8 months age group. There is no significant loss of DA
931 neurons in both ages. The estimated cell numbers in one hemisphere are shown. Data are
932 represented as mean ± SEM (Student's unpaired t-test). n=3 mice per genotype.

933 (C), (D) Tiling of a single coronal striatum section labelled for DAT in 2 months (C) SJ1 cKO^{DAT}
934 and (D) SJ1-KI^{RQ} mice. Unlike SJ1-KI^{RQ}, DAT clusters were observed in the entire striatum of
935 SJ1 cKO^{DAT} mice. Scale bar: 500 µm.

936 (E) Representative images of DAT immunostaining in the striatum of SJ1 cKO^{DAT} at 3 weeks,
937 2 months, 6 months and 12 months age group. Scale bar: 50 µm.

938

939 **Supplementary Figure 2. Other markers examined in the SJ1 cKO^{DAT} striatum**

940 (A) Immunostaining of vMAT2 with SV2C showed colocalization for clusters in the striatum of
941 2 months SJ1 cKO^{DAT} mice. Scale bar: 20 µm.

942 (B), (C) Immunostaining of DAT with (B) Syt1 and (C) alpha-Syn showed partial colocalization
943 with DAT-positive clusters in the striatum of 2 months SJ1 cKO^{DAT} mice. Scale bar: 20 µm.

944 (D) Immunostaining of DAT with pSer129-α-syn showed no misfolded alpha-Synuclein
945 accumulated in DAT-positive clusters in the striatum of 2 months SJ1 cKO^{DAT} mice. Scale bar:
946 20 µm.

947 (E), (F) Immunostaining of DAT with (E) D2R and (F) Darpp32 showed no colocalization with
948 DAT-positive clusters in the striatum of 2 months SJ1 cKO^{DAT} mice, suggesting there is no
949 effect on postsynaptic neurons. Scale bar: 20 µm.

950 (G), (H) Immunostaining of DAT with (G) GFAP and (H) Iba1 showed similar glia cell pattern
951 in both Ctrl and SJ1 cKO^{DAT} mice at 2 months old, suggesting there is no gliosis and
952 inflammation in the striatum. Scale bar: 20 µm.

953

954 **Supplementary Figure 3. Endocytic markers examined in the SJ1 cKO^{DAT} striatum**

955 (A)-(D) Double staining of DAT with (A) SJ1, (B) CLC, (C) amphiphysin 1 and (D) endophilin
956 1 showed no colocalization of these clathrin-related endocytic proteins with DAT-positive
957 clusters in the striatum of 2 months old SJ1 cKO^{DAT} mice. Scale bar: 20 μm.

958

959 **Supplementary Figure 4. More EM images of whirl-like membrane accumulation at DA**
960 **terminals in SJ1 cKO^{DAT} striatum.**

961 (A), (B) More representative EM images to show the abnormal lipid membrane accumulation
962 which is correlated with DAT/TH-positive protein clusters in 2 months old SJ1 cKO^{DAT} striatum.
963 Abnormal whirl-like multilayered membrane (red arrows) surrounding the synaptic vesicles
964 (SVs) and endosomes (endo). Mitochondria (mt) also labeled in the terminals. Scale bar:
965 200 nm and 500nm.

966

967 **Supplementary Figure 5. Western blot analysis of endocytic markers in the SJ1 cKO^{DAT}**
968 **striatum**

969 (A) Representative blots for endocytic markers, including SJ1, BIN1, Endophilin 1, Dynamin 1
970 and AP2 from 2-3 months old Ctrl and SJ1 cKO^{DAT} half brain striatal homogenates. The protein
971 expression levels of these endocytic factors remain unchanged.

972 (B) Quantification of proteins level shown in (A). Protein levels were normalized to the level of
973 actin. n=3-5 mice per genotype.

974

975 **Supplementary Figure 6. Distribution of iTHINs in whole striatum of SJ1 cKO^{DAT}**

976 (A) Tiling of a single coronal striatum section with TH immunostaining in 2 months old SJ1
977 cKO^{DAT} mice. Insets: TH-positive clusters and iTHINs were both observed throughout the
978 striatum, including dorsal striatum (DS), ventral striatum (VS) and olfactory tubercle (OT).
979 Scale bar: 500 μm.

980 (B) Representative images of TH immunostaining in the striatum of SJ1 cKO^{DAT} at 3 weeks, 2
981 months, 6 months and 12 months age group. TH-positive iTHINs (white arrows) and clusters
982 (asterisk) were labeled. Scale bar: 50 μm.

983

984 **Supplementary Figure 7. iTHINs are a distinct group of striatal interneurons**

985 (A)-(C) Immunostaining of TH with (A) NPY, (B) PV and (C) ChAT in SJ1 cKO^{DAT} striatum
986 showed that iTHINs is a distinct group of neurons from other striatal interneurons. Scale bar:
987 20 μm.

988 (D), (E) Very few iTHINs in the striatum of SJ1 cKO^{DAT} occasionally co-express (D) Calretinin
989 and (E) Darpp32, suggesting heterogeneity within iTHINs subpopulation. Scale bar: 20 μm.

990

991 **Supplementary Figure 8. A subpopulation of iTHINs in SJ1 cKO^{DAT} dorsal striatum**
992 **expresses ALDH1A1**

993 (A) Immunostaining of TH and ALDH1A1 in the midbrain of 2 months SJ1 cKO^{DAT} mice shows
994 the ventral tier DA neurons expressing ALDH1A1. Scale bar: 20 μm.

995 (B) Tiling of a single coronal striatum section immunostained for TH and ALDH1A1 of 2 months
996 old Ctrl and SJ1 cKO^{DAT} mice. TH/ALDH1A1-positive iTHINs were mainly distributed in dorsal
997 striatum (DS). Scale bar: 500 μm

998 (C) Immunostaining of TH and Calbindin in the midbrain of 2 months SJ1 cKO^{DAT} mice shows
999 some VTA DA neurons expressing Calbindin. Scale bar: 20 μm.

1000 (D) Immunostaining shows that iTHINs in the striatum of 2 months SJ1 cKO^{DAT} mice were
1001 negative for Calbindin. Scale bar: 50 μm.

1002

1003 **Supplementary Figure 9. Control AAV labeling for the specific DA-iTHINs connection**

1004 (A) Schematic showing experiment procedure and timeline. pAAV-FLEX-tdTomato (Cre-
1005 dependent) was injected unilaterally into the striatum of TH-Cre, DAT-Cre, SJ1 cKOTH and SJ1
1006 cKO^{DAT} mice at 2-3 months old. Animal brains were collected for IHC 2 weeks post injection.

1007 (B) Representative images of tdT expression and TH immunostaining in the injected striatum
1008 of SJ1 cKOTH and SJ1 cKO^{DAT} with their respective Cre line control, TH-Cre and DAT-Cre mice.
1009 In TH-Cre, tdT labeled WT THINs (red arrows) that were negative for anti-TH. In SJ1 cKOTH,
1010 TH immunostaining labeled all iTHINs (blue arrows), some tdT-expressing WT THINs (red
1011 arrow) and tdT expressing iTHINs (white arrow) were observed. No tdT-expressing neurons
1012 observed in DAT-Cre injected striatum. While TH immunostaining labeled all iTHINs (blue
1013 arrow), tdT specifically labeled some iTHINs (white arrow) in SJ1 cKO^{DAT} mice. Scale bar: 50
1014 μm.

1015 (C) Schematic showing experiment procedure and timeline. rAAV-mTH-EGFP was unilaterally
1016 in the midbrain of B6, Ai9;TH-Cre and Ai9;SJ1 cKOTH mice at 2-3 months old. Animal brains
1017 were collected 2 weeks post injection for IHC.

1018 (D) Representative images of EGFP expression, tdT expression and TH immunostaining in
1019 the striatum of injected mice. EGFP was not expressed in WT THINs (red arrows) in injected
1020 Ai9;TH-Cre mice. However, EGFP was expressed in TH/tdT-positive iTHINs (white arrows)
1021 but not TH-negative/tdT-positive WT THINs (red arrows) in Ai9;SJ1 cKOTH mice. This suggests
1022 EGFP labelling is specific to iTHINs in SJ1 cKO mice. Scale bar: 50 μm.

1023 (E) Schematic showing experiment procedure and timeline. pAAV-hSyn-mCherry was
1024 unilaterally injected into the striatum of B6 mice at 2-3 months old. Animal brains were
1025 collected 2 weeks post injection for IHC.

1026 (F) Representative images of mCherry expression and Darpp32 immunostaining in the
1027 striatum of injected mice. mCherry-positive neurons were randomly observed in the striatum
1028 of injected mice, with a subset of them positive for Darpp32 (white arrows). Scale bar: 50 μm.

1029

1030 **Supplementary Figure 10. Controls for lesioned models and Summary of iTHINs**

1031 (A) Representative striatum images of Ai9;DAT-Cre mice unilaterally injected with Casp3 (Cre-
1032 mediated) in the midbrain. THINs appearing in the striatum of lesioned model (white arrows)
1033 were not expressing tdT, indicating DAT gene promoter is not activated in lesioned model
1034 THINs. Scale bar: 200 μm.

1035 (B) Illustration summary of the new features of THINs induced in the SJ1 DA cKO striatum.

1036

1037 **Supplementary Figure 11. Controls for SJ1 Acute KO model**

1038 (A), (B) Representative images of (A) adult B6 mice (2 months old) and (B) aged B6 mice (12
1039 months old) unilaterally injected with AAV-TH-Cre virus show no loss of DA somata in the
1040 midbrain or DA fibers in the striatum, validating the safety and non-toxicity of AAV TH-Cre used.
1041 Scale bar: 200 μm.

1042

1043 **Supplementary Table 1. Comparison of THINs observed in WT, genetic SJ1 DA cKO and**
1044 **acute DA lesion mouse models**

1045 Immunostaining against TH, AADC, ALDH1A1 and DAT, and Cre-dependent labelling were
1046 performed to examine the gene/protein expression of these DA markers in THINs and iTHINs.

1047

1048

1049

1050

References

1. Bandres-Ciga, S., Diez-Fairen, M., Kim, J.J., and Singleton, A.B. (2020). Genetics of Parkinson's disease: An introspection of its journey towards precision medicine. Neurobiol Dis *137*, 104782. 10.1016/j.nbd.2020.104782.
2. Ng, X.Y., and Cao, M. (2024). Dysfunction of synaptic endocytic trafficking in Parkinson's disease. Neural Regen Res *19*, 2649-2660. 10.4103/NRR.NRR-D-23-01624.
3. Saheki, Y., and De Camilli, P. (2012). Synaptic vesicle endocytosis. Cold Spring Harbor perspectives in biology *4*, a005645. 10.1101/cshperspect.a005645.
4. Milosevic, I., Giovedi, S., Lou, X., Raimondi, A., Collesi, C., Shen, H., Paradise, S., O'Toole, E., Ferguson, S., Cremona, O., and De Camilli, P. (2011). Recruitment of Endophilin to Clathrin-Coated Pit Necks Is Required for Efficient Vesicle Uncoating after Fission. Neuron *72*, 587-601. 10.1016/j.neuron.2011.08.029.
5. Verstreken, P., Koh, T.-W., Schulze, K.L., Zhai, R.G., Hiesinger, P.R., Zhou, Y., Mehta, S.Q., Cao, Y., Roos, J., and Bellen, H.J. (2003). Synaptojanin Is Recruited by Endophilin to Promote Synaptic Vesicle Uncoating. Neuron *40*, 733-748. 10.1016/S0896-6273(03)00644-5.
6. Schuske, K.R., Richmond, J.E., Matthies, D.S., Davis, W.S., Runz, S., Rube, D.A., van der Bliek, A.M., and Jorgensen, E.M. (2003). Endophilin Is Required for Synaptic Vesicle Endocytosis by Localizing Synaptojanin. Neuron *40*, 749-762. 10.1016/S0896-6273(03)00667-6.
7. Hayashi, M., Raimondi, A., O'Toole, E., Paradise, S., Collesi, C., Cremona, O., Ferguson, S.M., and De Camilli, P. (2008). Cell- and stimulus-dependent heterogeneity of synaptic vesicle endocytic recycling mechanisms revealed by studies of dynamin 1-null neurons. Proc Natl Acad Sci U S A *105*, 2175-2180. 10.1073/pnas.0712171105.
8. Krebs, C.E., Karkheiran, S., Powell, J.C., Cao, M., Makarov, V., Darvish, H., Di Paolo, G., Walker, R.H., Shahidi, G.A., Buxbaum, J.D., et al. (2013). The Sac1 domain of SYNJ1 identified mutated in a family with early-onset progressive Parkinsonism with generalized seizures. Hum Mutat *34*, 1200-1207. 10.1002/humu.22372.
9. Quadri, M., Fang, M., Picillo, M., Olgiati, S., Breedveld, G.J., Graafland, J., Wu, B., Xu, F., Erro, R., Amboni, M., et al. (2013). Mutation in the SYNJ1 gene associated with autosomal recessive, early-onset Parkinsonism. Hum Mutat *34*, 1208-1215. 10.1002/humu.22373.
10. Lesage, S., Mangone, G., Tesson, C., Bertrand, H., Benmahdjoub, M., Kesraoui, S., Arezki, M., Singleton, A., Corvol, J.C., and Brice, A. (2021). Clinical Variability of SYNJ1-Associated Early-Onset Parkinsonism. Front Neurol *12*, 648457. 10.3389/fneur.2021.648457.
11. Dyment, D.A., Smith, A.C., Humphreys, P., Schwartzentruber, J., Beaulieu, C.L., Consortium, F.C., Bulman, D.E., Majewski, J., Woulfe, J., Michaud, J., and Boycott, K.M. (2015). Homozygous nonsense mutation in SYNJ1 associated with intractable epilepsy and tau pathology. Neurobiology of aging *36*, 1222 e1221-1225. 10.1016/j.neurobiolaging.2014.09.005.
12. Rauschendorf, M.A., Jost, M., Stock, F., Zimmer, A., Rosler, B., Rijntjes, M., Piroth, T., Coenen, V.A., Reinacher, P.C., Meyer, P.T., et al. (2017). Novel compound heterozygous synaptojanin-1 mutation causes l-dopa-responsive dystonia-parkinsonism syndrome. Mov Disord *32*, 478-480. 10.1002/mds.26876.
13. Senkevich, K., Parlar, S.C., Chantereault, C., Yu, E., Ahmad, J., Ruskey, J.A., Asayesh, F., Spiegelman, D., Waters, C., Monchi, O., et al. (2024). Are rare heterozygous SYNJ1 variants associated with Parkinson's disease? NPJ Parkinsons Dis *10*, 201. 10.1038/s41531-024-00809-9.

14. Farrow, S.L., Schierding, W., Gokuladhas, S., Golovina, E., Fadason, T., Cooper, A.A., and O'Sullivan, J.M. (2022). Establishing gene regulatory networks from Parkinson's disease risk loci. Brain *145*, 2422-2435. 10.1093/brain/awac022.
15. Gao, X., Huang, Z., Feng, C., Guan, C., Li, R., Xie, H., Chen, J., Li, M., Que, R., Deng, B., et al. (2020). Multimodal analysis of gene expression from postmortem brains and blood identifies synaptic vesicle trafficking genes to be associated with Parkinson's disease. Brief Bioinform. 10.1093/bib/bbaa244.
16. Cremona, O., Di Paolo, G., Wenk, M.R., Luthi, A., Kim, W.T., Takei, K., Daniell, L., Nemoto, Y., Shears, S.B., Flavell, R.A., et al. (1999). Essential role of phosphoinositide metabolism in synaptic vesicle recycling. Cell *99*, 179-188. S0092-8674(00)81649-9 [pii].
17. Pan, P.Y., Sheehan, P., Wang, Q., Zhu, X., Zhang, Y., Choi, I., Li, X., Saenz, J., Zhu, J., Wang, J., et al. (2020). Synj1 haploinsufficiency causes dopamine neuron vulnerability and alpha-synuclein accumulation in mice. Hum Mol Genet *29*, 2300-2312. 10.1093/hmg/ddaa080.
18. Zhu, X., Prakash, S.S., McAuliffe, G., and Pan, P.Y. (2023). Synaptojanin1 Modifies Endolysosomal Parameters in Cultured Ventral Midbrain Neurons. eneuro *10*. 10.1523/ENEURO.0426-22.2023.
19. Pan, P.-Y., Zhu, J., Rizvi, A., Zhu, X., Tanaka, H., and Dreyfus, C.F. (2021). Synaptojanin1 deficiency upregulates basal autophagosome formation in astrocytes. Journal of Biological Chemistry *297*. 10.1016/j.jbc.2021.100873.
20. Cao, M., Wu, Y., Ashrafi, G., McCartney, A.J., Wheeler, H., Bushong, E.A., Boassa, D., Ellisman, M.H., Ryan, T.A., and De Camilli, P. (2017). Parkinson Sac Domain Mutation in Synaptojanin 1 Impairs Clathrin Uncoating at Synapses and Triggers Dystrophic Changes in Dopaminergic Axons. Neuron *93*, 882-896 e885. 10.1016/j.neuron.2017.01.019.
21. Ng, X.Y., Wu, Y., Lin, Y., Yaqoob, S.M., Greene, L.E., De Camilli, P., Cao, M., and (2023). Mutations in Parkinsonism-linked endocytic proteins synaptojanin1 and auxilin have synergistic effects on dopaminergic axonal pathology. npj Parkinson's Disease *9*. 10.1038/s41531-023-00465-5.
22. Nalls, M.A., Pankratz, N., Lill, C.M., Do, C.B., Hernandez, D.G., Saad, M., DeStefano, A.L., Kara, E., Bras, J., Sharma, M., et al. (2014). Large-scale meta-analysis of genome-wide association data identifies six new risk loci for Parkinson's disease. Nature Genetics *46*, 989-993. 10.1038/ng.3043.
23. Cao, M., Park, D., Wu, Y., and De Camilli, P. (2020). Absence of Sac2/INPP5F enhances the phenotype of a Parkinson's disease mutation of synaptojanin 1. Proc Natl Acad Sci U S A *117*, 12428-12434. 10.1073/pnas.2004335117.
24. Pan, P.Y., Li, X., Wang, J., Powell, J., Wang, Q., Zhang, Y., Chen, Z., Wicinski, B., Hof, P., Ryan, T.A., and Yue, Z. (2017). Parkinson's Disease-Associated LRRK2 Hyperactive Kinase Mutant Disrupts Synaptic Vesicle Trafficking in Ventral Midbrain Neurons. J Neurosci *37*, 11366-11376. 10.1523/JNEUROSCI.0964-17.2017.
25. Tashiro, Y., Sugimoto, T., Hattori, T., Uemura, Y., Nagatsu, I., Kikuchi, H., and Mizuno, N. (1989). Tyrosine hydroxylase-like immunoreactive neurons in the striatum of the rat. Neuroscience Letters *97*, 6-10. doi.org/10.1016/0304-3940(89)90130-4.
26. Nakahara, T., Yamamoto, T., Endo, K., and Kayama, H. (2001). Neuronal ectopic expression of tyrosine hydroxylase in the mouse striatum by combined administration of 1-methyl-4-phenyl-1,2,3,6-tetrahydropyridine and 3-nitropropionic acid. Neuroscience *108*, 601-610. doi.org/10.1016/S0306-4522(01)00441-9.
27. Ibáñez-Sandoval, O., Tecuapetla, F., Unal, B., Shah, F., Koós, T., and Tepper, J.M. (2010). Electrophysiological and Morphological Characteristics and Synaptic Connectivity of Tyrosine Hydroxylase-Expressing Neurons in Adult Mouse Striatum. The Journal of Neuroscience *30*, 6999-7016. 10.1523/JNEUROSCI.5996-09.2010.
28. Dubach, M., Schmidt, R., Kunkel, D., Bowden, D.M., Martin, R., and German, D.C. (1987). Primate neostriatal neurons containing tyrosine hydroxylase:

Immunohistochemical evidence. Neuroscience Letters *75*, 205-210. doi.org/10.1016/0304-3940(87)90298-9.

29. Betarbet, R., Turner, R., Chockkan, V., DeLong, M.R., Allers, K.A., Walters, J., Levey, A.I., and Greenamyre, J.T. (1997). Dopaminergic neurons intrinsic to the primate striatum. J Neurosci *17*, 6761-6768. 10.1523/JNEUROSCI.17-17-06761.1997.
30. Porritt, M.J., Batchelor, P.E., Hughes, A.J., Kalnins, R., Donnan, G.A., and Howells, D.W. (2000). New dopaminergic neurons in Parkinson's disease striatum. Lancet *356*, 44-45. 10.1016/S0140-6736(00)02437-5.
31. Cossette, M., Lecomte, F., and Parent, A. (2005). Morphology and distribution of dopaminergic neurons intrinsic to the human striatum. J Chem Neuroanat *29*, 1-11. 10.1016/j.jchemneu.2004.08.007.
32. Huot, P., Levesque, M., and Parent, A. (2006). The fate of striatal dopaminergic neurons in Parkinson's disease and Huntington's chorea. Brain *130*, 222-232. 10.1093/brain/awl332.
33. Xenias, H.S., Ibáñez-Sandoval, O., Koós, T., and Tepper, J.M. (2015). Are Striatal Tyrosine Hydroxylase Interneurons Dopaminergic? The Journal of Neuroscience *35*, 6584-6599. 10.1523/JNEUROSCI.0195-15.2015.
34. Tepper, J.M., Koós, T., Ibanez-Sandoval, O., Tecuapetla, F., Faust, T.W., and Assous, M. (2018). Heterogeneity and Diversity of Striatal GABAergic Interneurons: Update 2018. Frontiers in Neuroanatomy *12*, 91. 10.3389/fnana.2018.00091.
35. Darmopil, S., Muñetón-Gómez, V.C., De Ceballos, M.L., Bernson, M., and Moratalla, R. (2008). Tyrosine hydroxylase cells appearing in the mouse striatum after dopamine denervation are likely to be projection neurones regulated by l-DOPA. European Journal of Neuroscience *27*, 580-592. 10.1111/j.1460-9568.2008.06040.x.
36. Masuda, M., Miura, M., Inoue, R., Imanishi, M., Saino-Saito, S., Takada, M., Kobayashi, K., and Aosaki, T. (2011). Postnatal development of tyrosine hydroxylase mRNA-expressing neurons in mouse neostriatum. European Journal of Neuroscience *34*, 1355-1367. 10.1111/j.1460-9568.2011.07873.x.
37. Mao, M., Nair, A., and Augustine, G.J. (2019). A Novel Type of Neuron Within the Dorsal Striatum. Frontiers in Neural Circuits *13*, 32. 10.3389/fncir.2019.00032.
38. Cai, H., Liu, G., Sun, L., and Ding, J. (2014). Aldehyde Dehydrogenase 1 making molecular inroads into the differential vulnerability of nigrostriatal dopaminergic neuron subtypes in Parkinson's disease. Translational Neurodegeneration *3*, 27. 10.1186/2047-9158-3-27.
39. Anderegg, A., Poulin, J.-F., and Awatramani, R. (2015). Molecular heterogeneity of midbrain dopaminergic neurons – Moving toward single cell resolution. FEBS Letters *589*, 3714-3726. doi.org/10.1016/j.febslet.2015.10.022.
40. Palfi, S., Leventhal, L., Chu, Y., Ma, S.Y., Emborg, M., Bakay, R., Déglon, N., Hantraye, P., Aebischer, P., and Kordower, J.H. (2002). Lentivirally Delivered Glial Cell Line-Derived Neurotrophic Factor Increases the Number of Striatal Dopaminergic Neurons in Primate Models of Nigrostriatal Degeneration. The Journal of Neuroscience *22*, 4942. 10.1523/JNEUROSCI.22-12-04942.2002.
41. Tande, D., Hoglinger, G., Debeir, T., Freundlieb, N., Hirsch, E.C., and Francois, C. (2006). New striatal dopamine neurons in MPTP-treated macaques result from a phenotypic shift and not neurogenesis. Brain *129*, 1194-1200. 10.1093/brain/awl041.
42. Ünal, B., Shah, F., Kothari, J., and Tepper, J.M. (2015). Anatomical and electrophysiological changes in striatal TH interneurons after loss of the nigrostriatal dopaminergic pathway. Brain Structure and Function *220*, 331-349. 10.1007/s00429-013-0658-8.
43. Troshev, D., Bannikova, A., Blokhin, V., Pavlova, E., Kolacheva, A., and Ugrumov, M. (2023). Compensatory Processes in Striatal Neurons Expressing the Tyrosine Hydroxylase Gene in Transgenic Mice in a Model of Parkinson's Disease. International Journal of Molecular Sciences *24*, 16245. 10.3390/ijms242216245.

44. Erben, L., Welday, J.P., Murphy, R., and Buonanno, A. (2022). Toxic and Phenotypic Effects of AAV_Cre Used to Transduce Mesencephalic Dopaminergic Neurons. International Journal of Molecular Sciences *23*. 10.3390/ijms23169462.
45. Rezai Amin, S., Gruszczynski, C., Guiard, B.P., Callebert, J., Launay, J.-M., Louis, F., Betancur, C., Vialou, V., and Gautron, S. (2019). Viral vector-mediated Cre recombinase expression in substantia nigra induces lesions of the nigrostriatal pathway associated with perturbations of dopamine-related behaviors and hallmarks of programmed cell death. Journal of Neurochemistry *150*, 330-340. doi.org/10.1111/jnc.14684.
46. Özçete, Ö.D., Banerjee, A., and Kaeser, P.S. (2024). Mechanisms of neuromodulatory volume transmission. Molecular Psychiatry *29*, 3680-3693. 10.1038/s41380-024-02608-3.
47. Chanaday, N.L., Cousin, M.A., Milosevic, I., Watanabe, S., and Morgan, J.R. (2019). The Synaptic Vesicle Cycle Revisited: New Insights into the Modes and Mechanisms. The Journal of Neuroscience *39*, 8209. 10.1523/JNEUROSCI.1158-19.2019.
48. Mejaes, J.I., Saenz, J., O'Brien, C., Pizzano, C.M., Pan, P.Y., and Barker, D.J. (2024). Haploinsufficiency of the Parkinson's disease gene synaptojanin1 is associated with abnormal responses to psychomotor stimulants and mesolimbic dopamine signaling. Front Behav Neurosci *18*, 1359225. 10.3389/fnbeh.2024.1359225.
49. Delignat-Lavaud, B., Kano, J., Ducrot, C., Masse, I., Mukherjee, S., Giguere, N., Moquin, L., Levesque, C., Burke, S., Denis, R., et al. (2023). Synaptotagmin-1-dependent phasic axonal dopamine release is dispensable for basic motor behaviors in mice. Nat Commun *14*, 4120. 10.1038/s41467-023-39805-7.
50. Cai, X., Liu, C., Tsutsui-Kimura, I., Lee, J.-H., Guo, C., Banerjee, A., Lee, J., Amo, R., Xie, Y., Patriarchi, T., et al. (2024). Dopamine dynamics are dispensable for movement but promote reward responses. Nature *635*, 406-414. 10.1038/s41586-024-08038-z.
51. Troshev, D., Bannikova, A., Blokhin, V., Kolacheva, A., Pronina, T., and Ugrumov, M. (2022). Striatal Neurons Partially Expressing a Dopaminergic Phenotype: Functional Significance and Regulation. International Journal of Molecular Sciences *23*, 11054. 10.3390/ijms231911054.
52. Rice, M.E., Patel, J.C., and Cragg, S.J. (2011). Dopamine release in the basal ganglia. Neuroscience *198*, 112-137. 10.1016/j.neuroscience.2011.08.066.
53. Ramírez-Jarquín, U.N., Sharma, M., Shahani, N., Li, Y., Boregowda, S., and Subramaniam, S. (2022). Rhes protein transits from neuron to neuron and facilitates mutant huntingtin spreading in the brain. Science Advances *8*, eabm3877. 10.1126/sciadv.abm3877.
54. Rufino-Ramos, D., Leandro, K., Perdigão, P.R.L., O'Brien, K., Pinto, M.M., Santana, M.M., van Solinge, T.S., Mahjoum, S., Breakefield, X.O., Breyne, K., and Pereira de Almeida, L. (2023). Extracellular communication between brain cells through functional transfer of Cre mRNA mediated by extracellular vesicles. Molecular Therapy *31*, 2220-2239. 10.1016/j.ymthe.2023.05.012.
55. Busceti, C.L., Bucci, D., Molinaro, G., Di Pietro, P., Zangrandi, L., Gradini, R., Moratalla, R., Battaglia, G., Bruno, V., Nicoletti, F., and Fornai, F. (2012). Lack or Inhibition of Dopaminergic Stimulation Induces a Development Increase of Striatal Tyrosine Hydroxylase-Positive Interneurons. PloS one *7*, e44025. 10.1371/journal.pone.0044025.

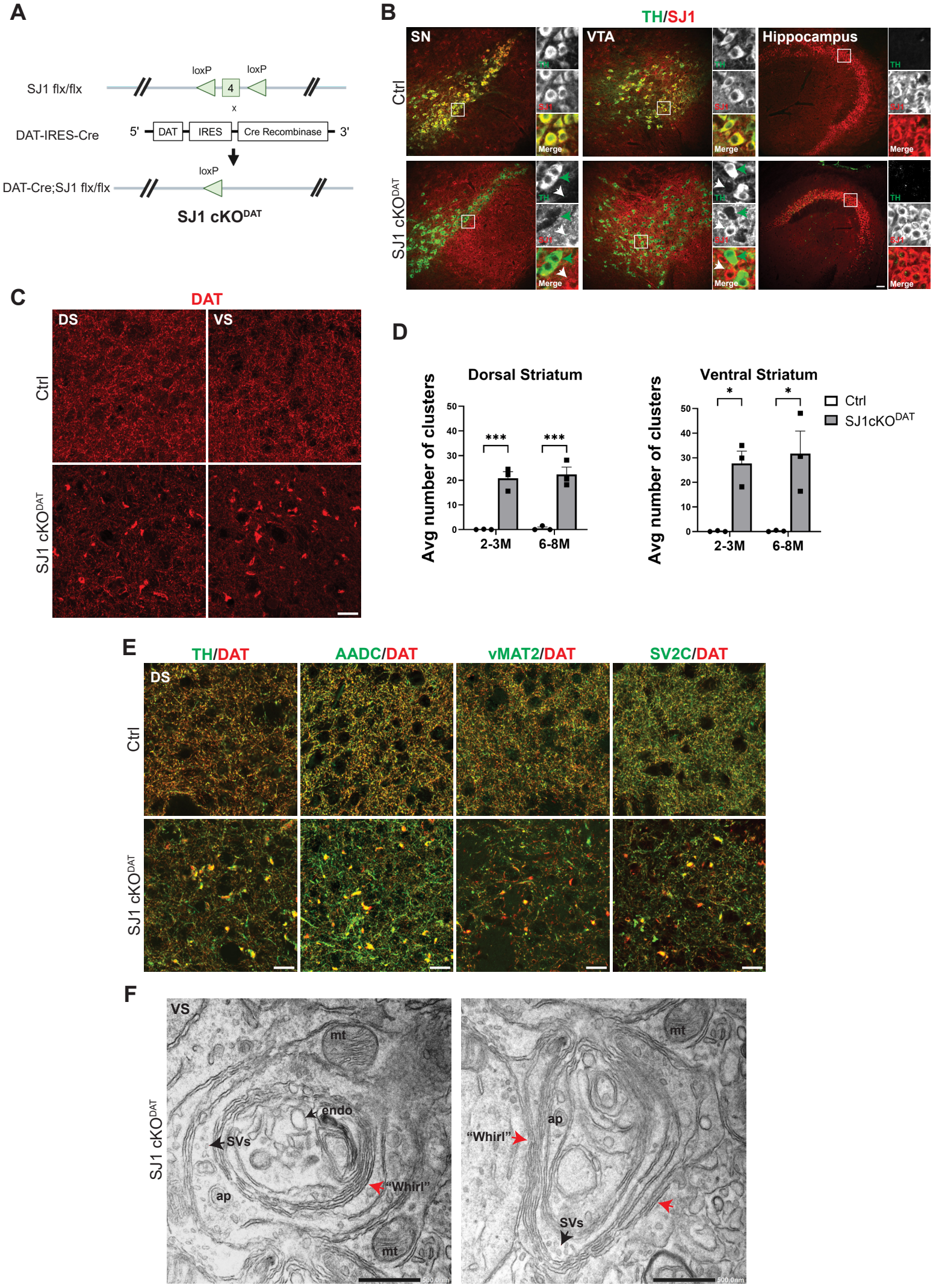
A
SJ1 flx/flx
loxP
loxP
4
x
DAT-IRES-Cre
5'
DAT
IRES
Cre Recombinase
3'
loxP
DAT-Cre;SJ1 flx/flx
SJ1 cKO^DAT
B
TH/SJ1
SN
VTA
Hippocampus
Ctrl
SJ1 cKO^DAT
TH
SJ1
Merge
C
DAT
DS
VS
Ctrl
SJ1 cKO^DAT
D
Dorsal Striatum
Avg number of clusters
***
***
2-3M
6-8M
Ventral Striatum
*
*
Ctrl
SJ1cKO^DAT
E
TH/DAT
AADC/DAT
vMAT2/DAT
SV2C/DAT
DS
Ctrl
SJ1 cKO^DAT
F
VS
mt
endo
SVs
ap
"Whirl"
mt
SJ1 cKO^DAT
ap
"Whirl"
SVs
500.0nm
500.0nm

Figure 1

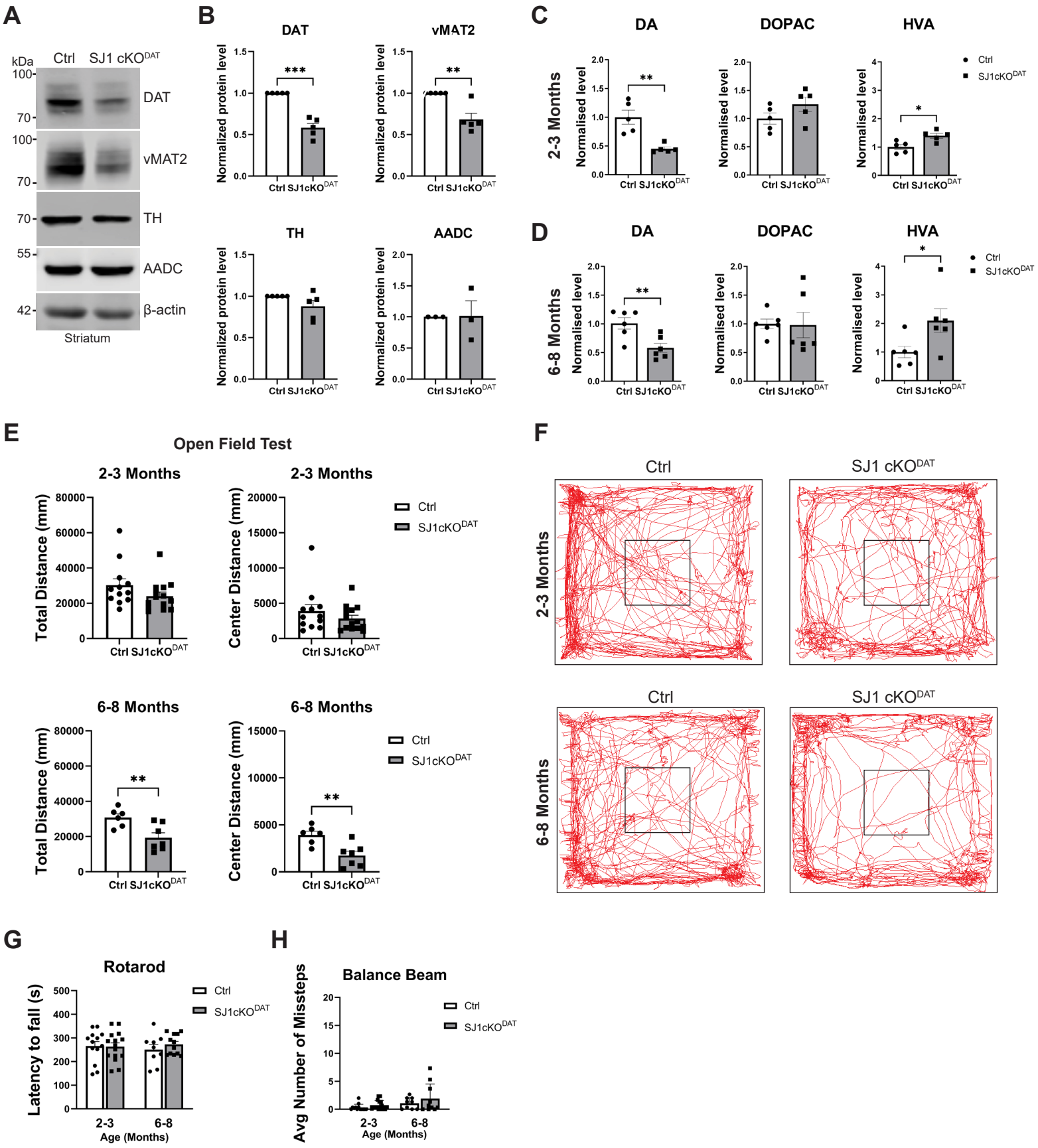
A
kDa
Ctrl
SJ1 cKO^{DAT}
100
70
DAT
100
70
vMAT2
70
TH
55
AADC
42
β-actin
Striatum
B
DAT
vMAT2
TH
AADC
Normalized protein level
Ctrl SJ1cKO^{DAT}
C
DA
DOPAC
HVA
2-3 Months
Normalised level
Ctrl
SJ1cKO^{DAT}
D
6-8 Months
E
Open Field Test
2-3 Months
6-8 Months
Total Distance (mm)
Center Distance (mm)
F
Ctrl
SJ1 cKO^{DAT}
2-3 Months
6-8 Months
G
Rotarod
Latency to fall (s)
Age (Months)
H
Balance Beam
Avg Number of Missteps

Figure 2

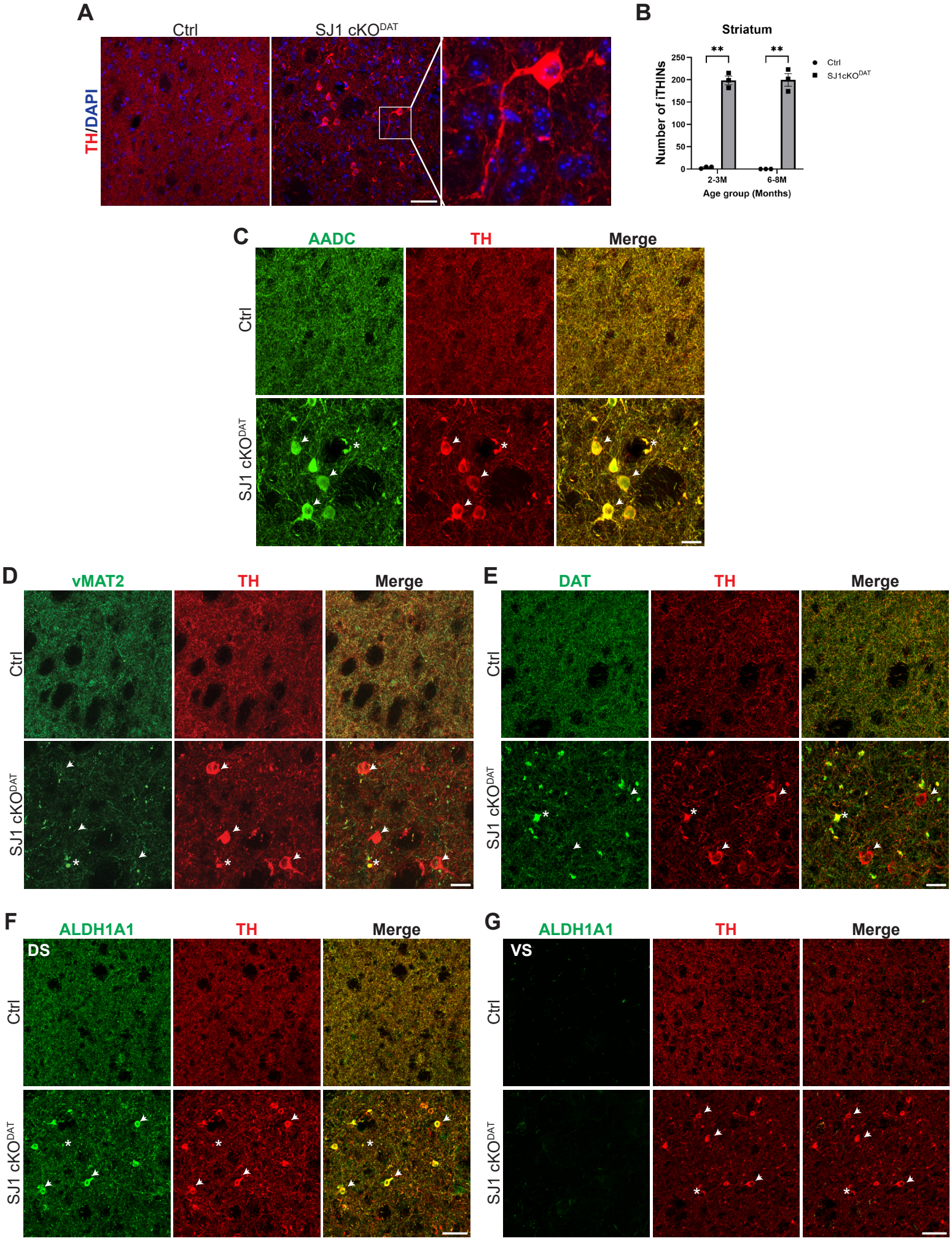
A
Ctrl
SJ1 cKO^DAT
TH/DAPI
B
Striatum
Number of iTHINs
Age group (Months)
2-3M
6-8M
Ctrl
SJ1cKO^DAT
C
AADC
TH
Merge
Ctrl
SJ1 cKO^DAT
D
vMAT2
TH
Merge
E
DAT
F
ALDH1A1
DS
G
VS

Figure 3

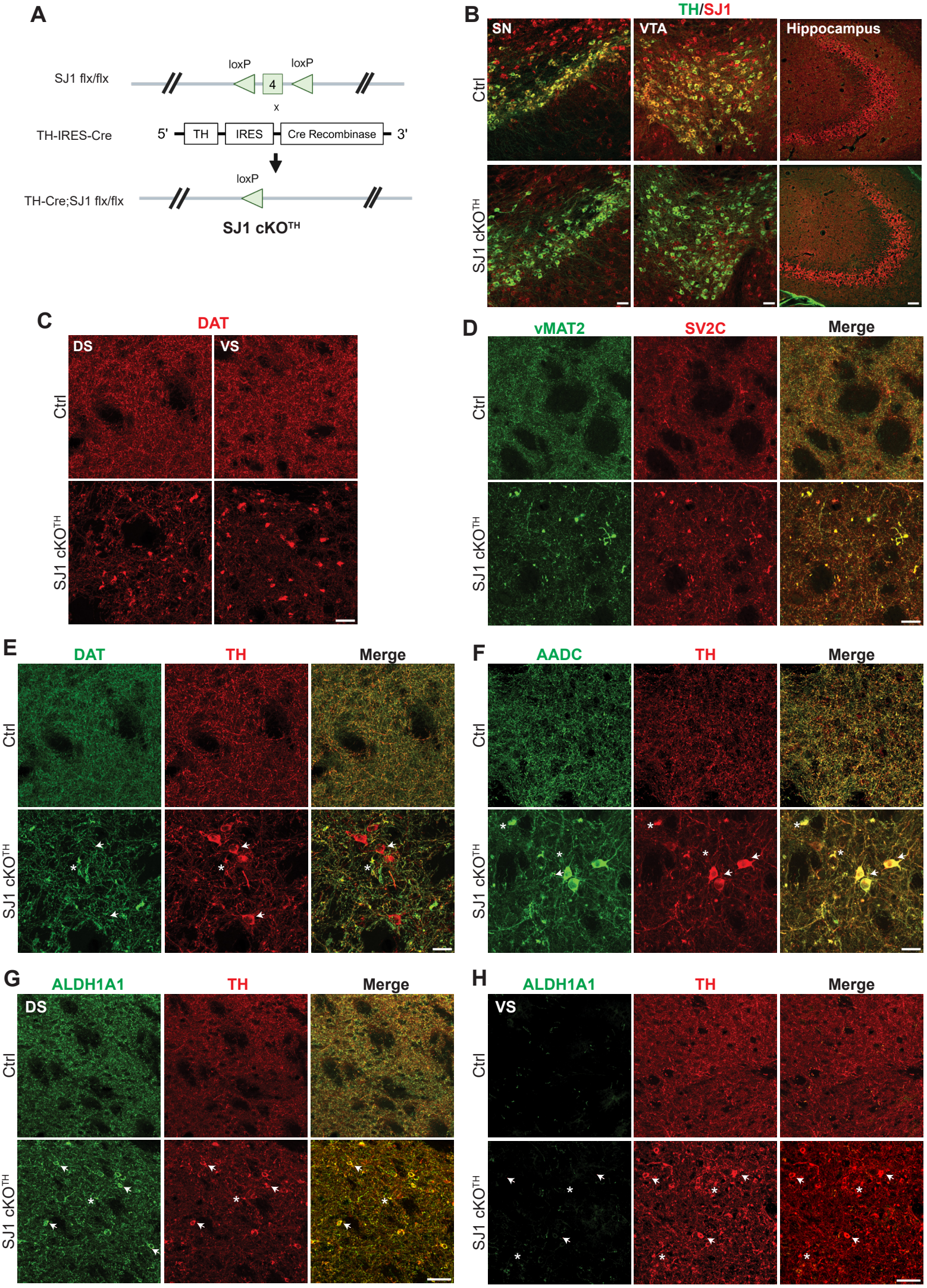
A
SJ1 flx/flx
loxP
loxP
4
x
TH-IRES-Cre
5'
TH
IRES
Cre Recombinase
3'
loxP
TH-Cre;SJ1 flx/flx
SJ1 cKO^TH
B
TH/SJ1
SN
VTA
Hippocampus
Ctrl
SJ1 cKO^TH
C
DAT
DS
VS
Ctrl
SJ1 cKO^TH
D
vMAT2
SV2C
Merge
Ctrl
SJ1 cKO^TH
E
DAT
TH
Merge
Ctrl
SJ1 cKO^TH
F
AADC
TH
Merge
Ctrl
SJ1 cKO^TH
G
ALDH1A1
TH
Merge
DS
Ctrl
SJ1 cKO^TH
H
ALDH1A1
TH
Merge
VS
Ctrl
SJ1 cKO^TH

Figure 4

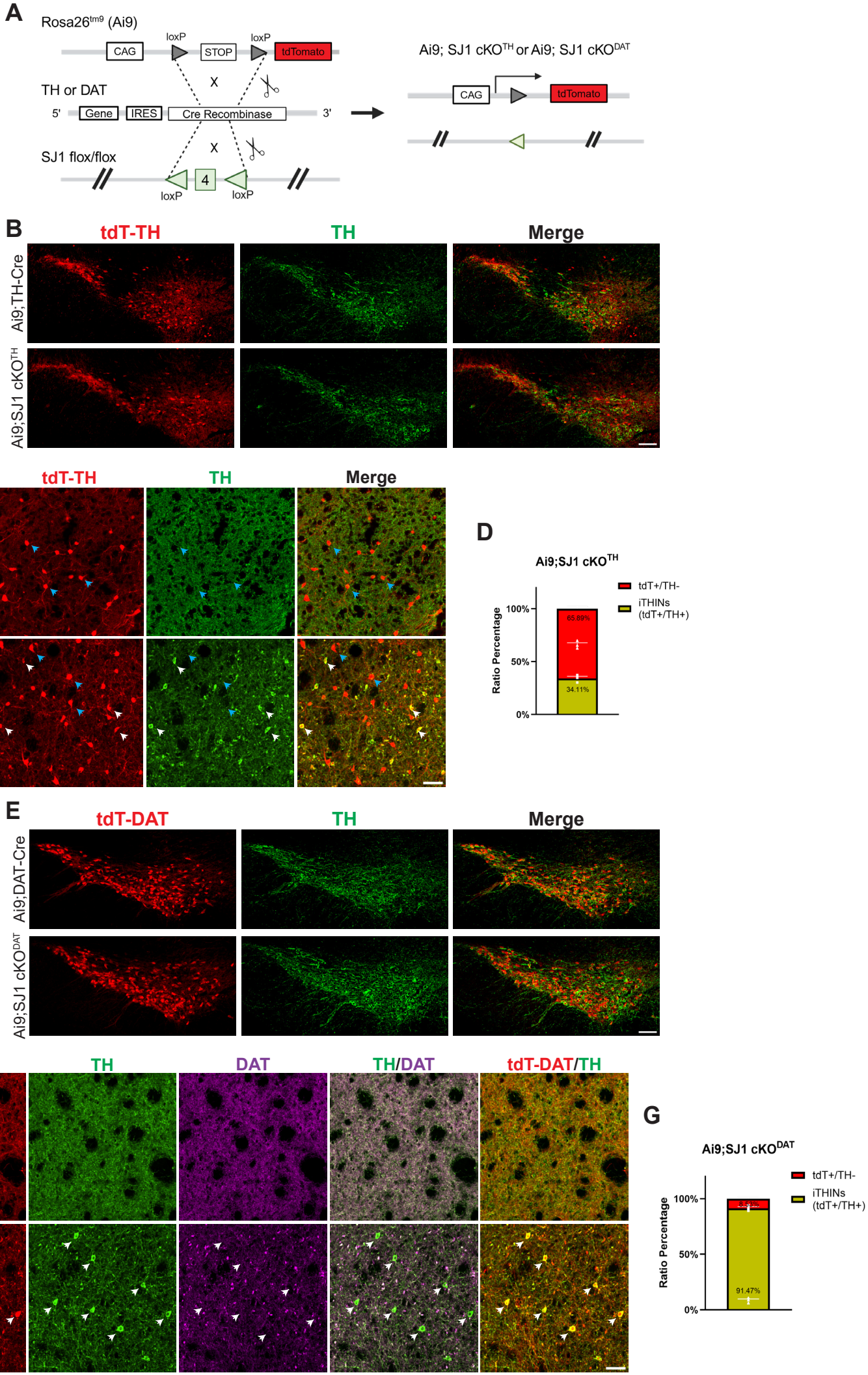
A
Rosa26tm9 (Ai9)
CAG
loxP
STOP
loxP
tdTomato
TH or DAT
5'
Gene
IRES
Cre Recombinase
3'
SJ1 flox/flox
loxP
4
loxP
Ai9; SJ1 cKOTH or Ai9; SJ1 cKODAT
CAG
tdTomato
B
tdT-TH
TH
Merge
Ai9;TH-Cre
Ai9;SJ1 cKOTH
C
tdT-TH
TH
Merge
Ai9;TH-Cre
Ai9;SJ1 cKOTH
D
Ai9;SJ1 cKOTH
tdT+/TH-
iTHINs (tdT+/TH+)
Ratio Percentage
100%
50%
0%
65.89%
34.11%
E
tdT-DAT
TH
Merge
Ai9;DAT-Cre
Ai9;SJ1 cKODAT
F
tdT-DAT
TH
DAT
TH/DAT
tdT-DAT/TH
Ai9; DAT-Cre
Ai9;SJ1 cKODAT
G
Ai9;SJ1 cKODAT
tdT+/TH-
iTHINs (tdT+/TH+)
Ratio Percentage
100%
50%
0%
91.47%

Figure 5

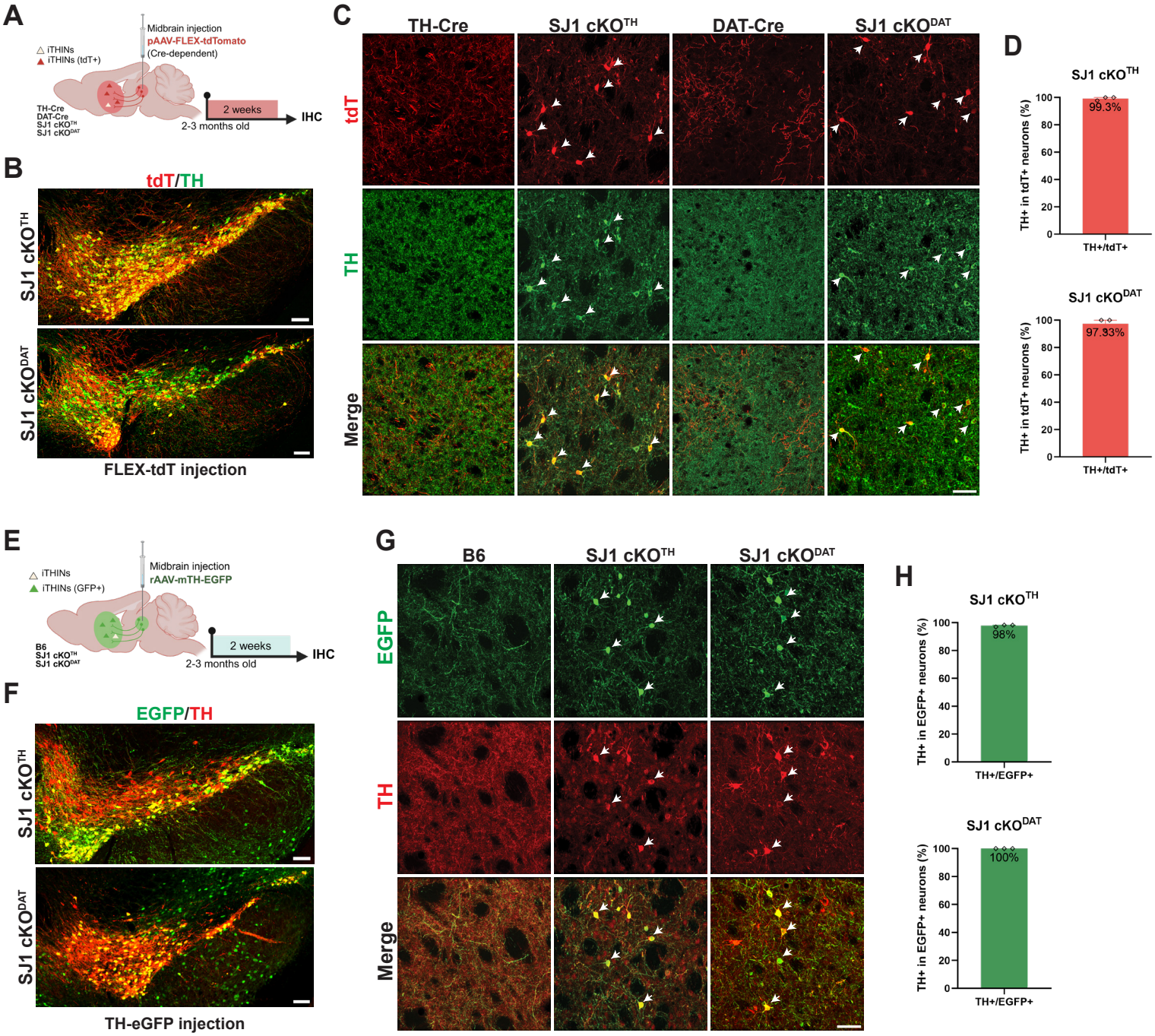
A
Midbrain injection
pAAV-FLEX-tdTomato
(Cre-dependent)
iTHINs
iTHINs (tdT+)
TH-Cre
DAT-Cre
SJ1 cKO^TH
SJ1 cKO^DAT
2 weeks
2-3 months old
IHC
B
tdT/TH
SJ1 cKO^TH
SJ1 cKO^DAT
FLEX-tdT injection
C
TH-Cre
SJ1 cKO^TH
DAT-Cre
SJ1 cKO^DAT
tdT
TH
Merge
D
SJ1 cKO^TH
99.3%
SJ1 cKO^DAT
97.33%
TH+ in tdT+ neurons (%)
TH+/tdT+
E
Midbrain injection
rAAV-mTH-EGFP
iTHINs
iTHINs (GFP+)
B6
SJ1 cKO^TH
SJ1 cKO^DAT
2 weeks
2-3 months old
IHC
F
EGFP/TH
SJ1 cKO^TH
SJ1 cKO^DAT
TH-eGFP injection
G
B6
SJ1 cKO^TH
SJ1 cKO^DAT
EGFP
TH
Merge
H
SJ1 cKO^TH
98%
SJ1 cKO^DAT
100%
TH+ in EGFP+ neurons (%)
TH+/EGFP+
I
Midbrain injection
pAAV-hSyn-mCherry
iTHINs
iTHINs (Cherry+)
B6
SJ1 cKO^TH
SJ1 cKO^DAT
2 weeks
2-3 months old
IHC
J
mCherry/TH
SJ1 cKO^TH
SJ1 cKO^DAT
hSyn-mCherry injection
K
B6
SJ1 cKO^TH
SJ1 cKO^DAT
mCherry
TH
Merge
L
SJ1 cKO^TH
94.8%
SJ1 cKO^DAT
92.6%
TH+ in mCherry+ neurons (%)
TH+/mCherry+

Figure 6

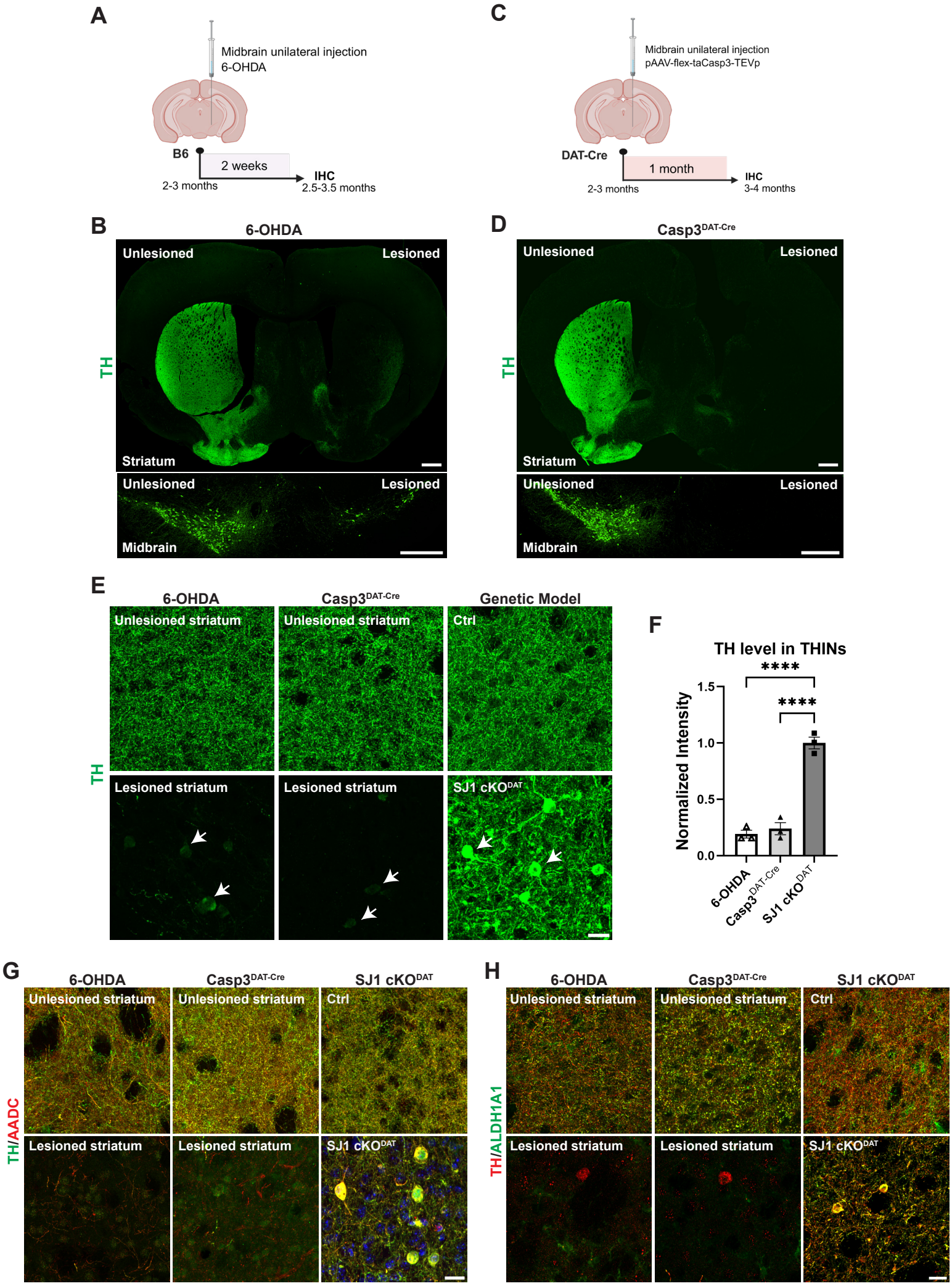
A
Midbrain unilateral injection
6-OHDA
B6
2 weeks
IHC
2-3 months
2.5-3.5 months
C
Midbrain unilateral injection
pAAV-flex-taCasp3-TEVp
DAT-Cre
1 month
IHC
2-3 months
3-4 months
B
6-OHDA
Unlesioned
Lesioned
TH
Striatum
Unlesioned
Lesioned
Midbrain
D
Casp3DAT-Cre
Unlesioned
Lesioned
TH
Striatum
Unlesioned
Lesioned
Midbrain
E
6-OHDA
Casp3DAT-Cre
Genetic Model
Unlesioned striatum
Unlesioned striatum
Ctrl
TH
Lesioned striatum
Lesioned striatum
SJ1 cKODAT
F
TH level in THINs
****
****
Normalized Intensity
1.5
1.0
0.5
0.0
6-OHDA
Casp3DAT-Cre
SJ1 cKODAT
G
6-OHDA
Casp3DAT-Cre
SJ1 cKODAT
Unlesioned striatum
Unlesioned striatum
Ctrl
TH/AADC
Lesioned striatum
Lesioned striatum
SJ1 cKODAT
H
6-OHDA
Casp3DAT-Cre
SJ1 cKODAT
Unlesioned striatum
Unlesioned striatum
Ctrl
TH/ALDH1A1
Lesioned striatum
Lesioned striatum
SJ1 cKODAT

Figure 7

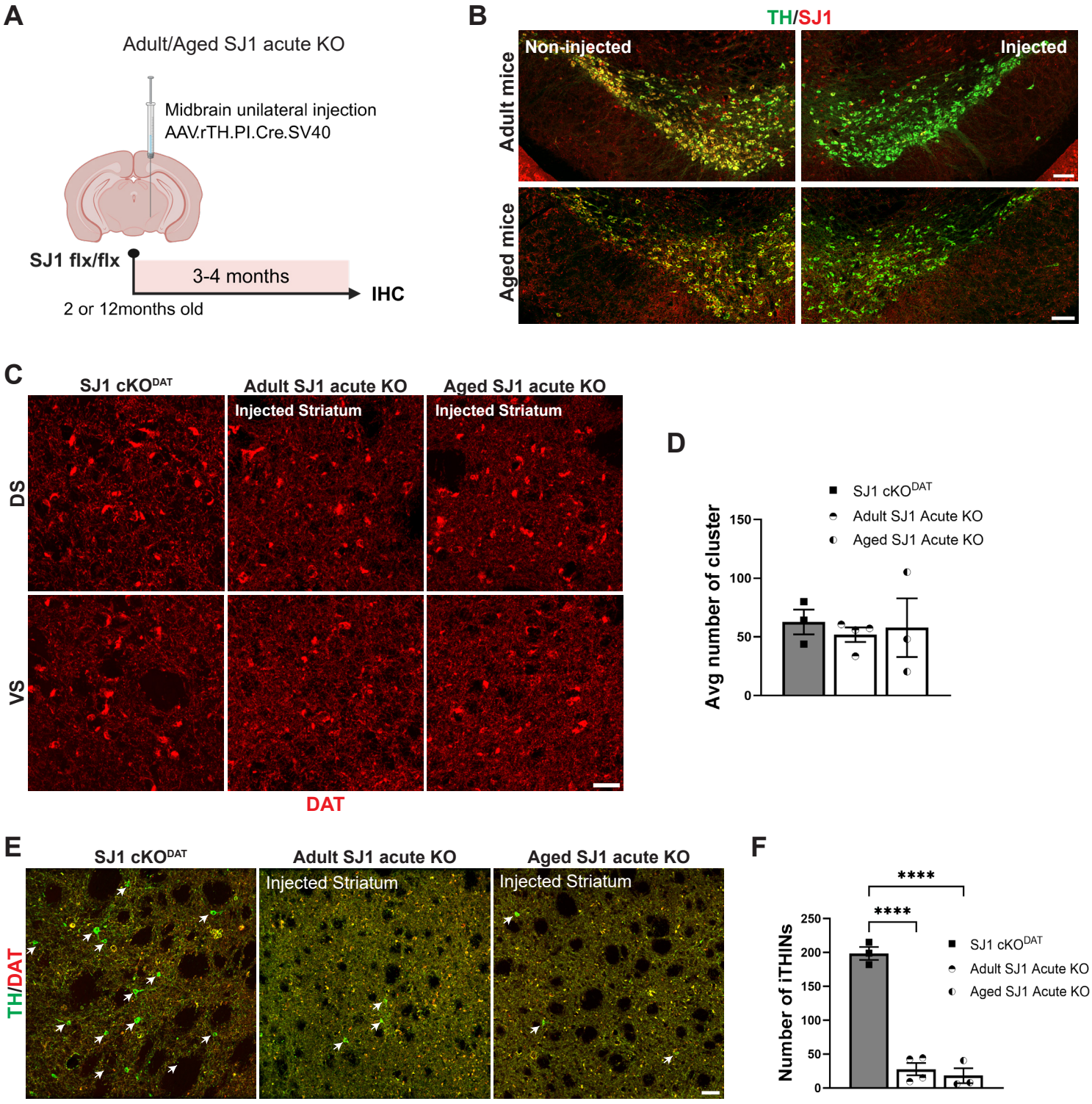
A
Adult/Aged SJ1 acute KO
Midbrain unilateral injection
AAV.rTH.PI.Cre.SV40
SJ1 flx/flx
3-4 months
IHC
2 or 12months old
B
TH/SJ1
Non-injected
Injected
Adult mice
Aged mice
C
SJ1 cKO^DAT
Adult SJ1 acute KO
Aged SJ1 acute KO
Injected Striatum
Injected Striatum
DS
VS
DAT
D
SJ1 cKO^DAT
Adult SJ1 Acute KO
Aged SJ1 Acute KO
Avg number of cluster
150
100
50
0
E
SJ1 cKO^DAT
Adult SJ1 acute KO
Aged SJ1 acute KO
Injected Striatum
Injected Striatum
TH/DAT
F
****
****
Number of iTHINs
250
200
150
100
50
0
SJ1 cKO^DAT
Adult SJ1 Acute KO
Aged SJ1 Acute KO

Figure 8

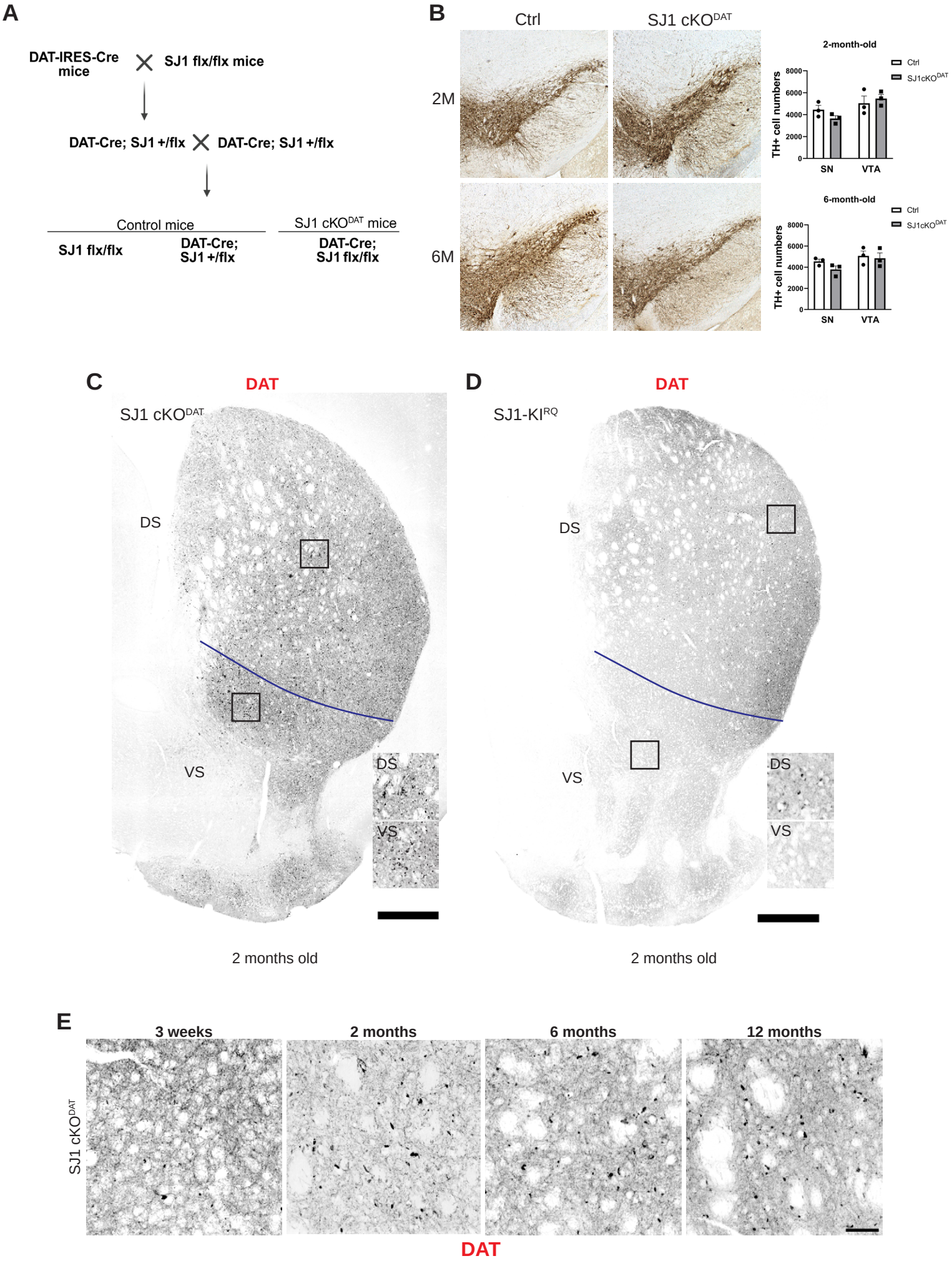

Supplementary Figure 1

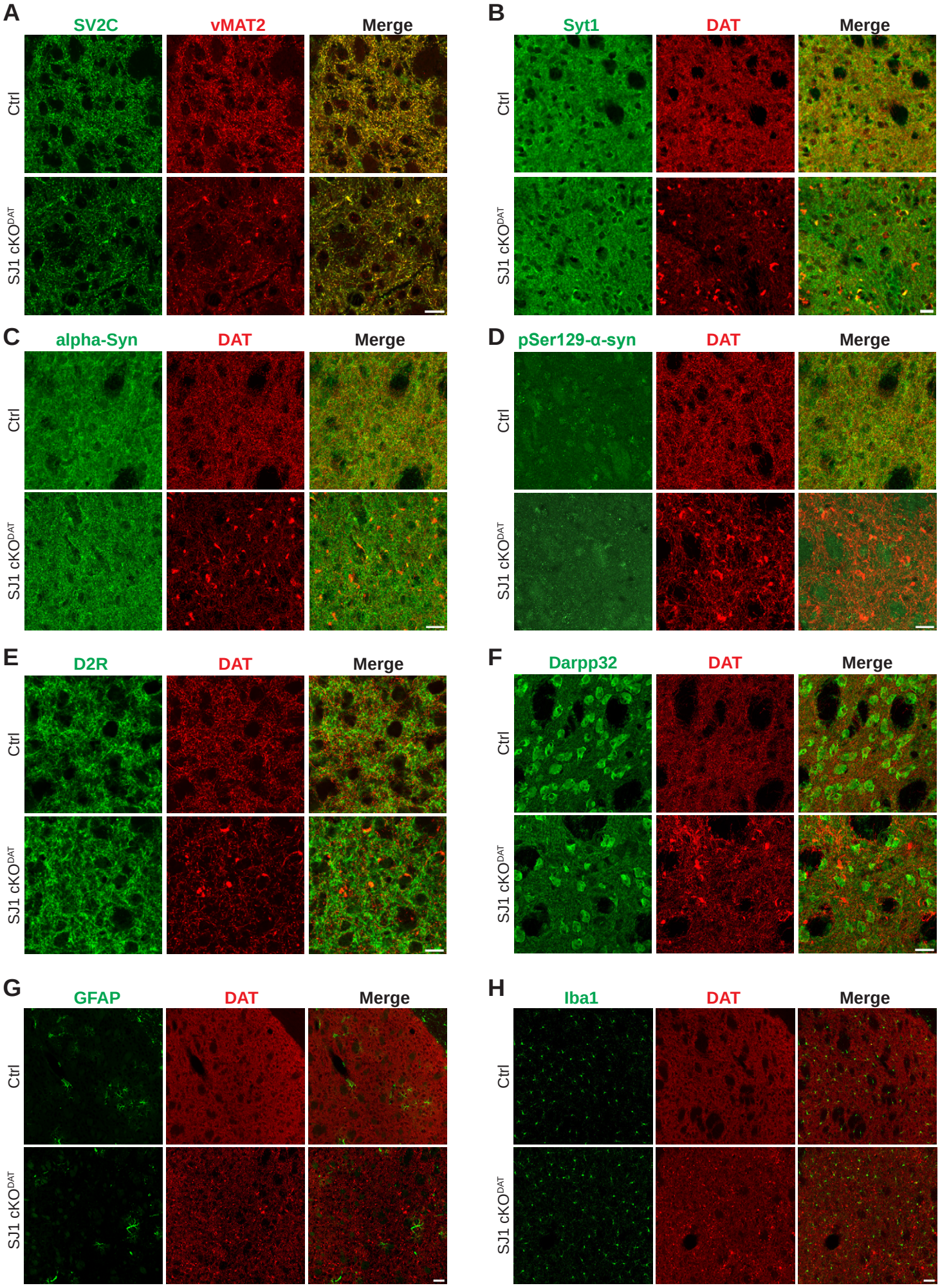

Supplementary Figure 2

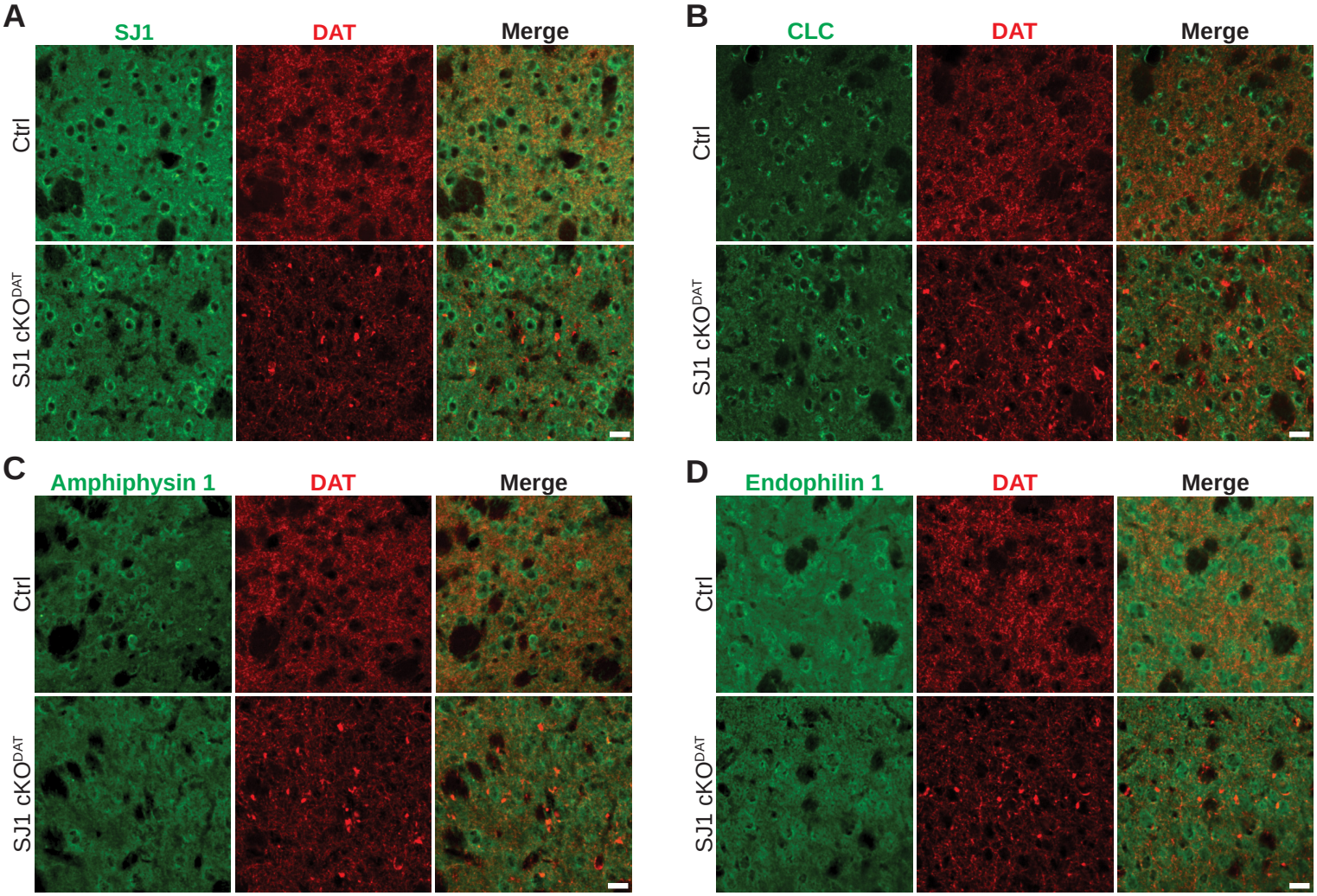

Supplementary Figure 3

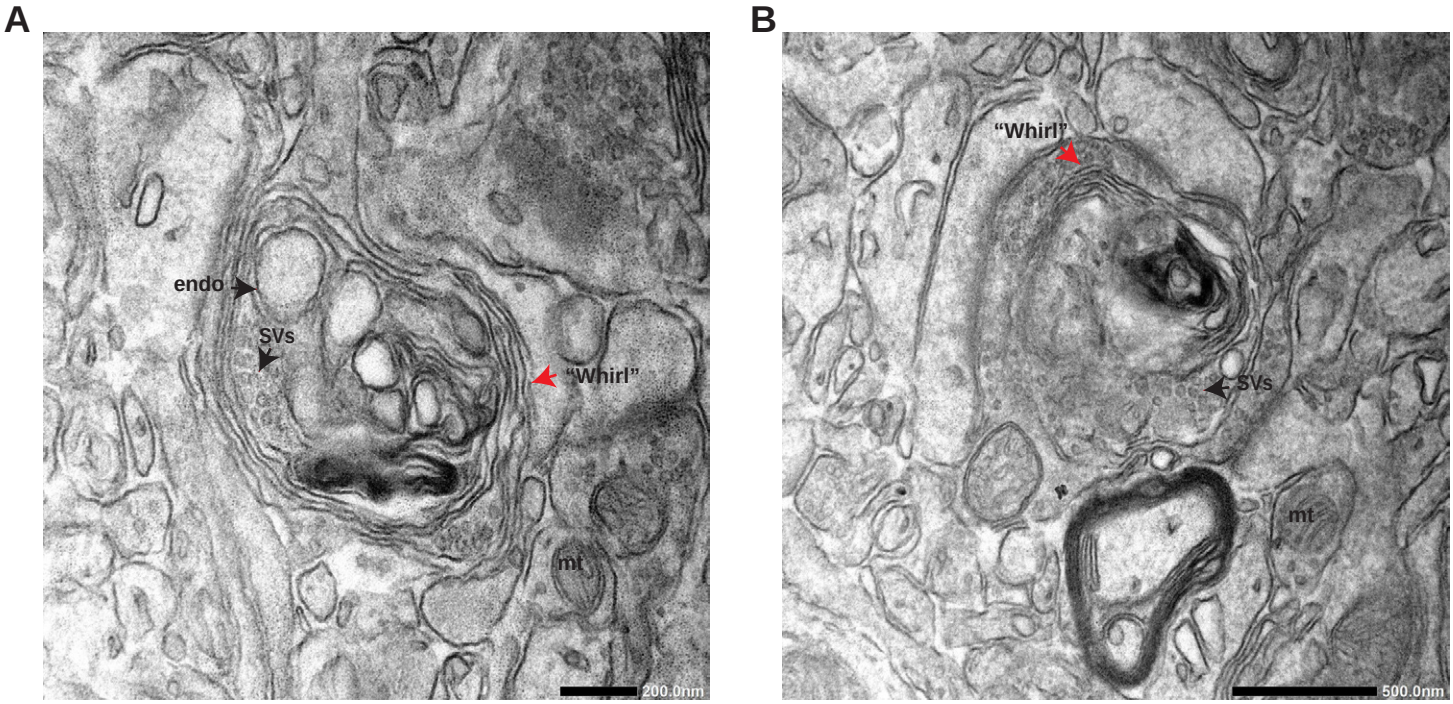

Supplementary Figure 4

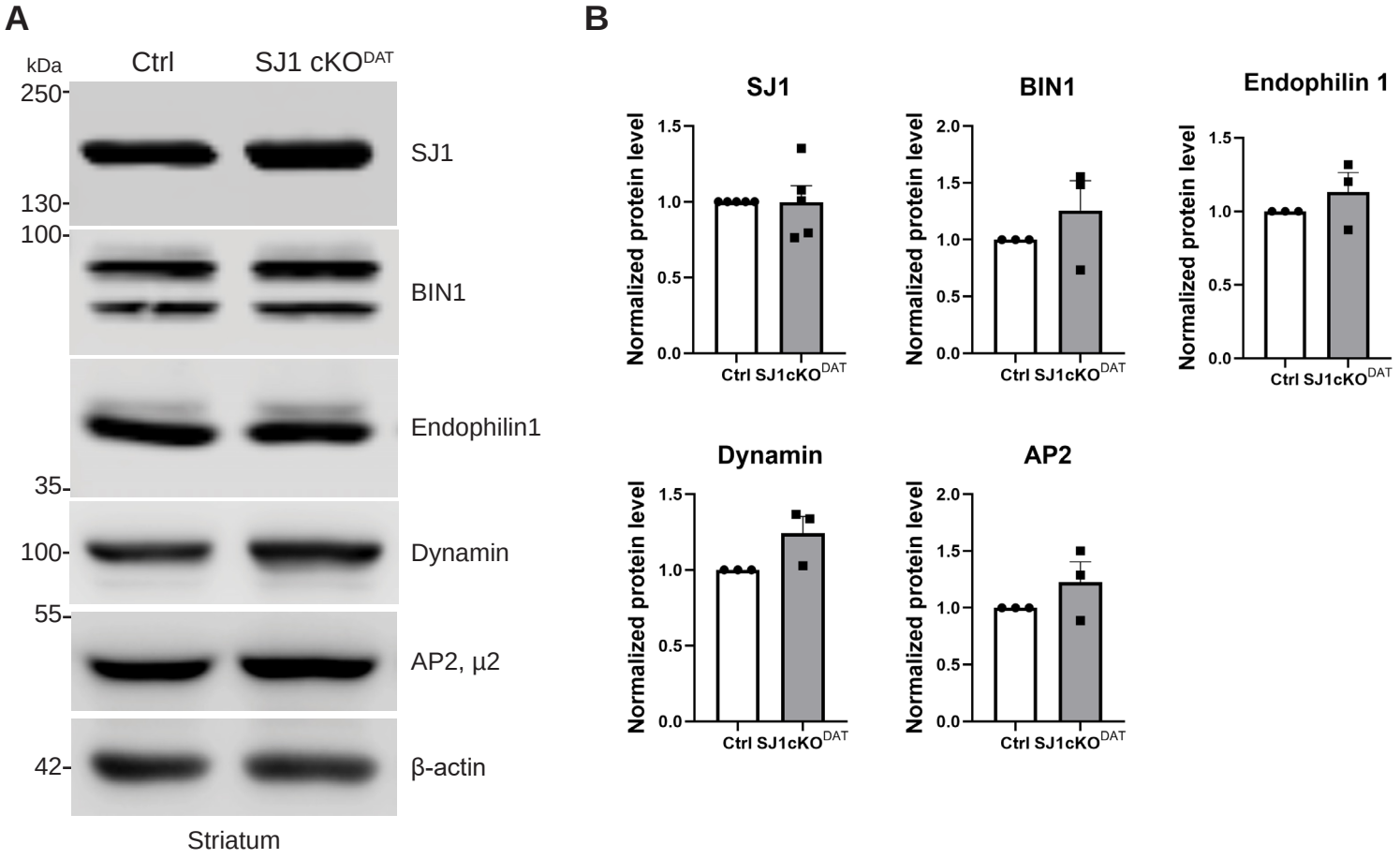

Supplementary Figure 5

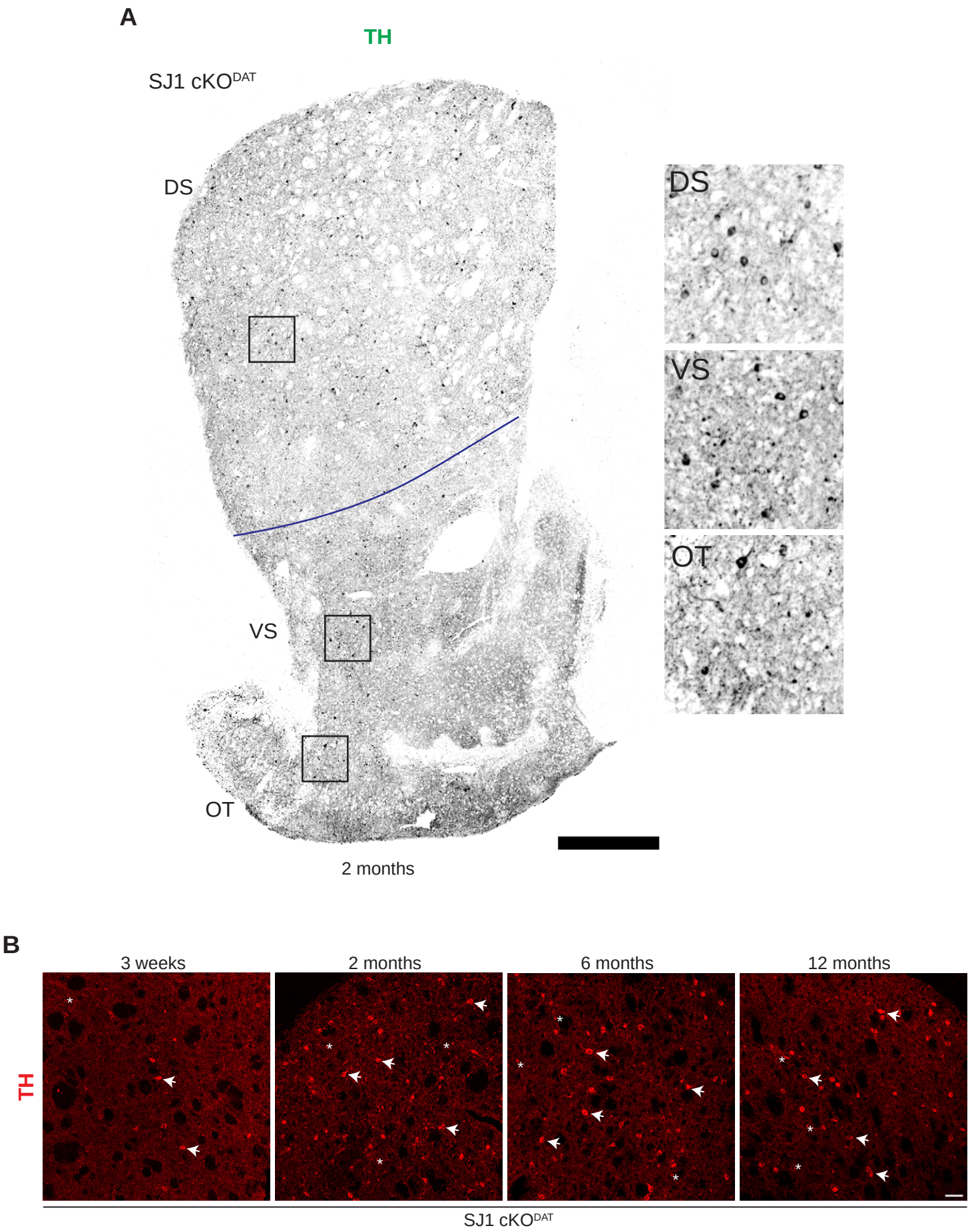

Supplementary Figure 6

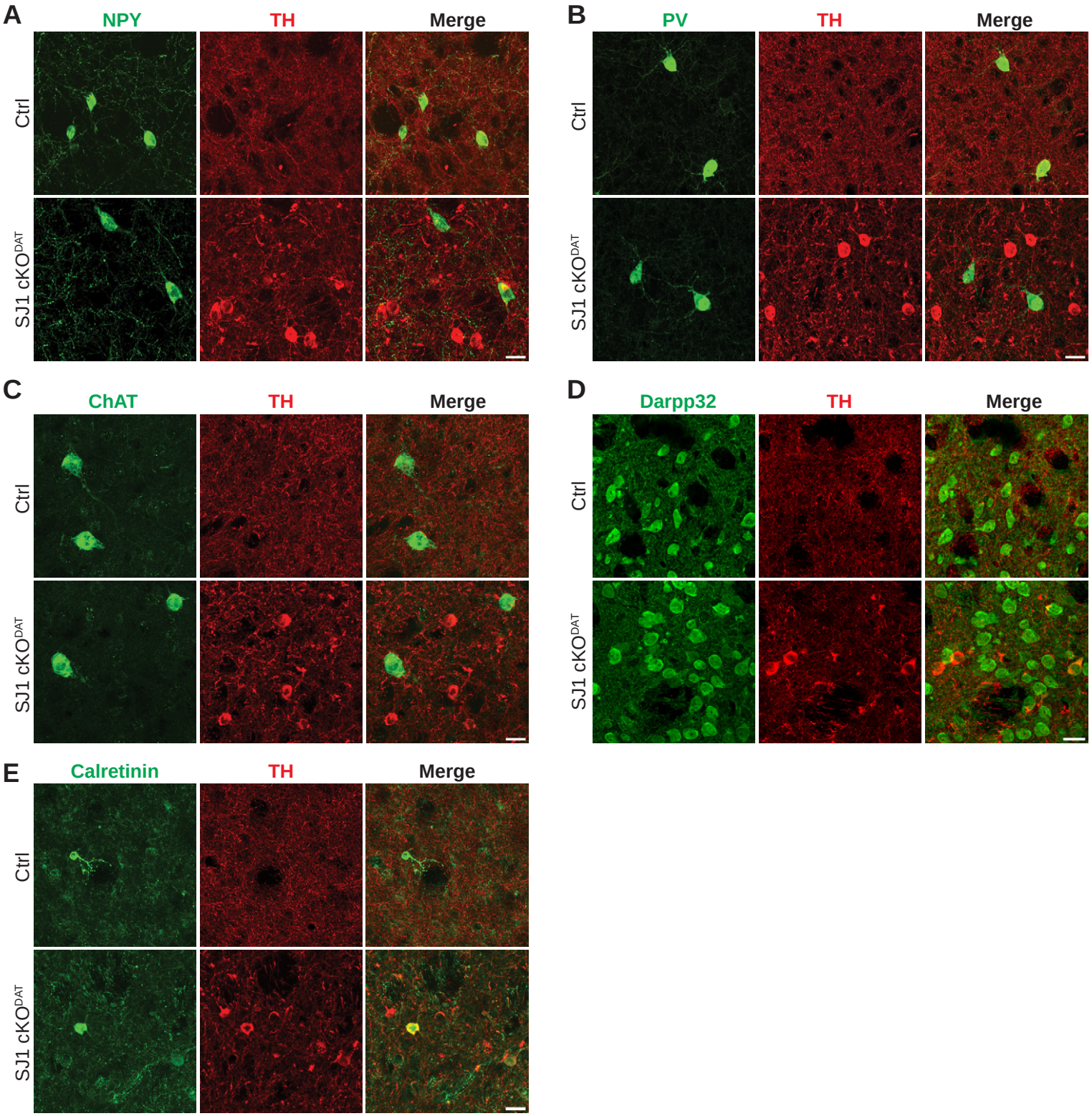

Supplementary Figure 7

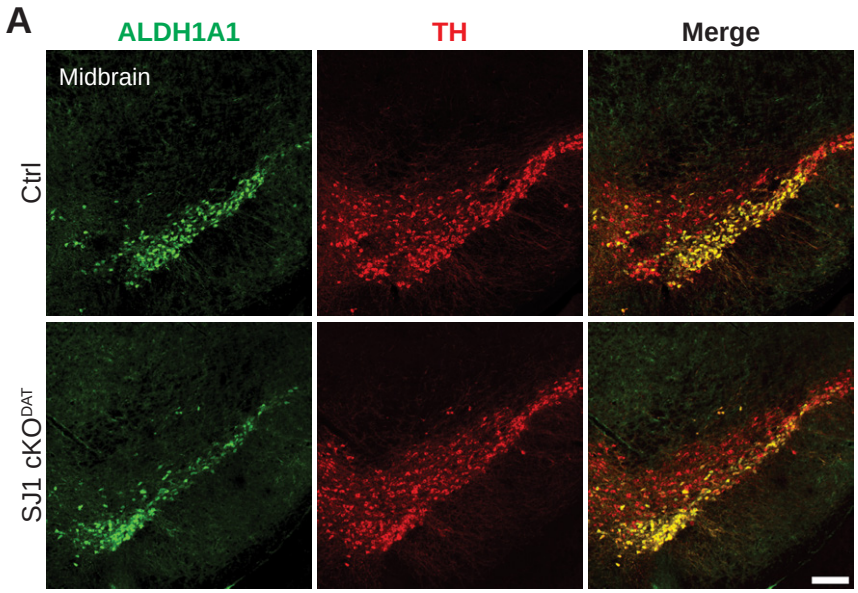

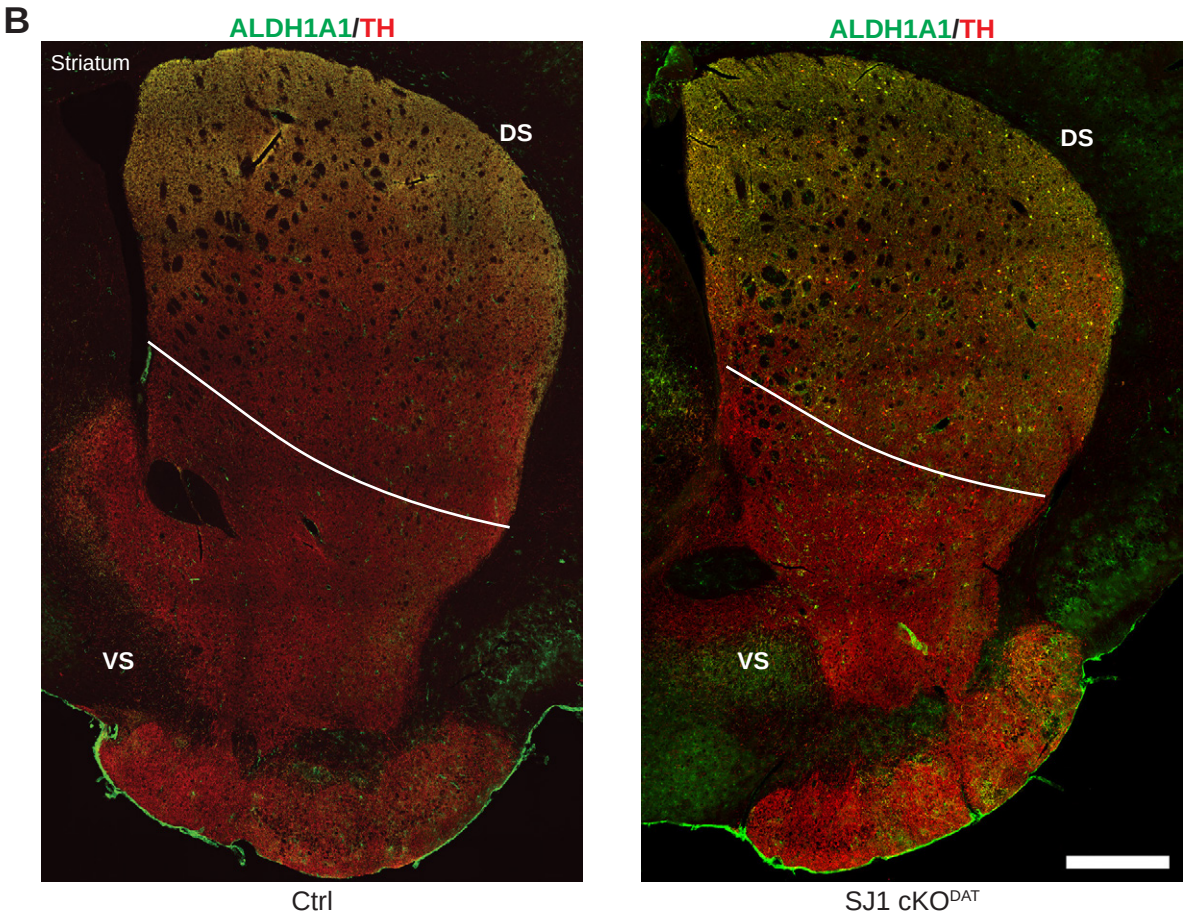

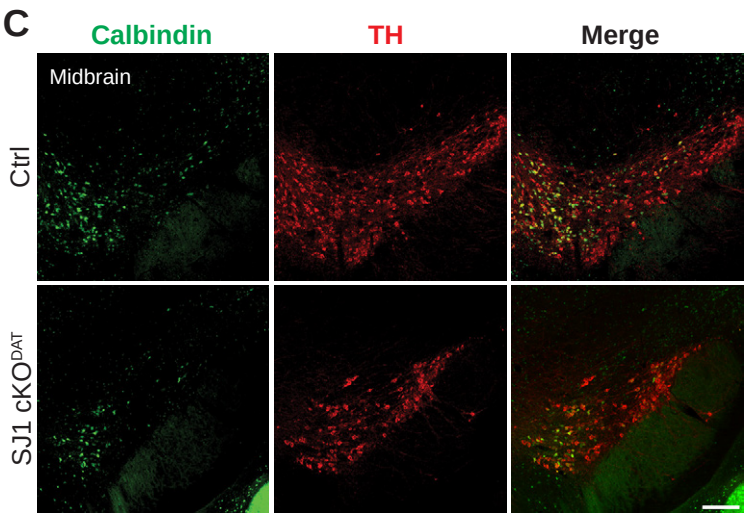

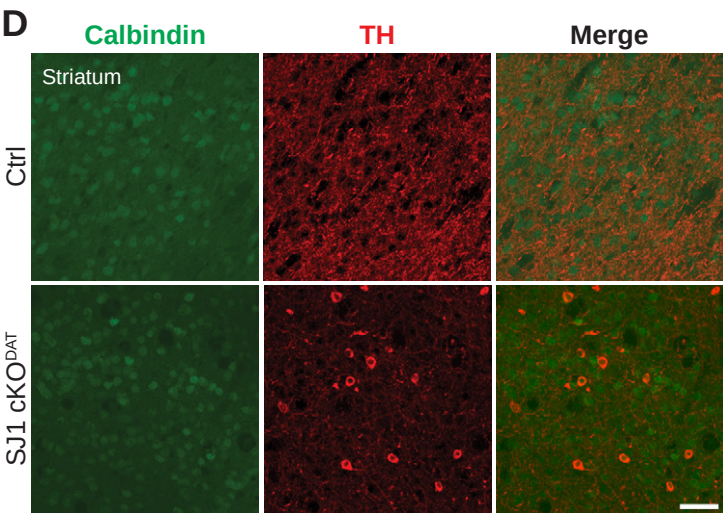

Supplementary Figure 8

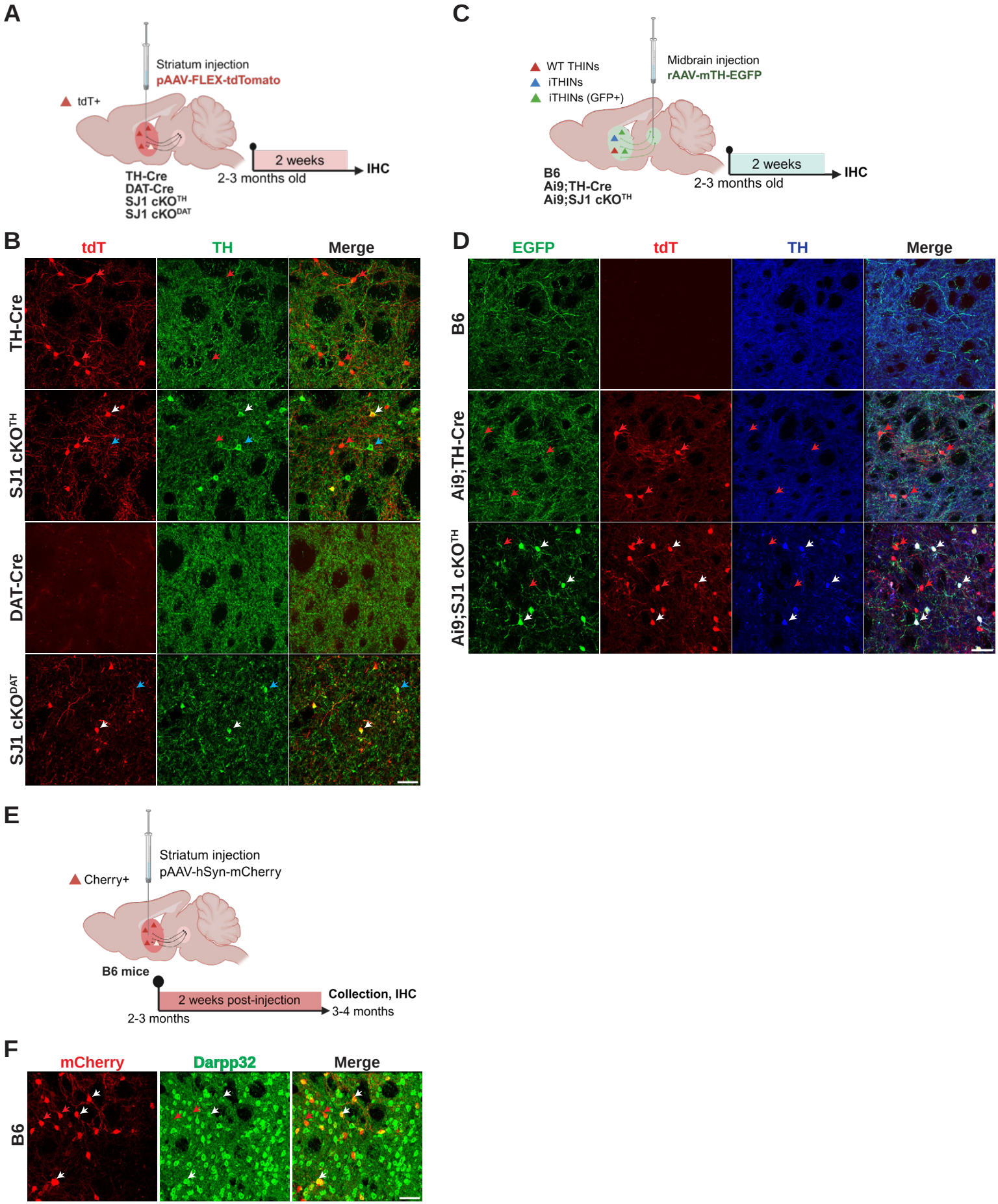

Supplementary Figure 9

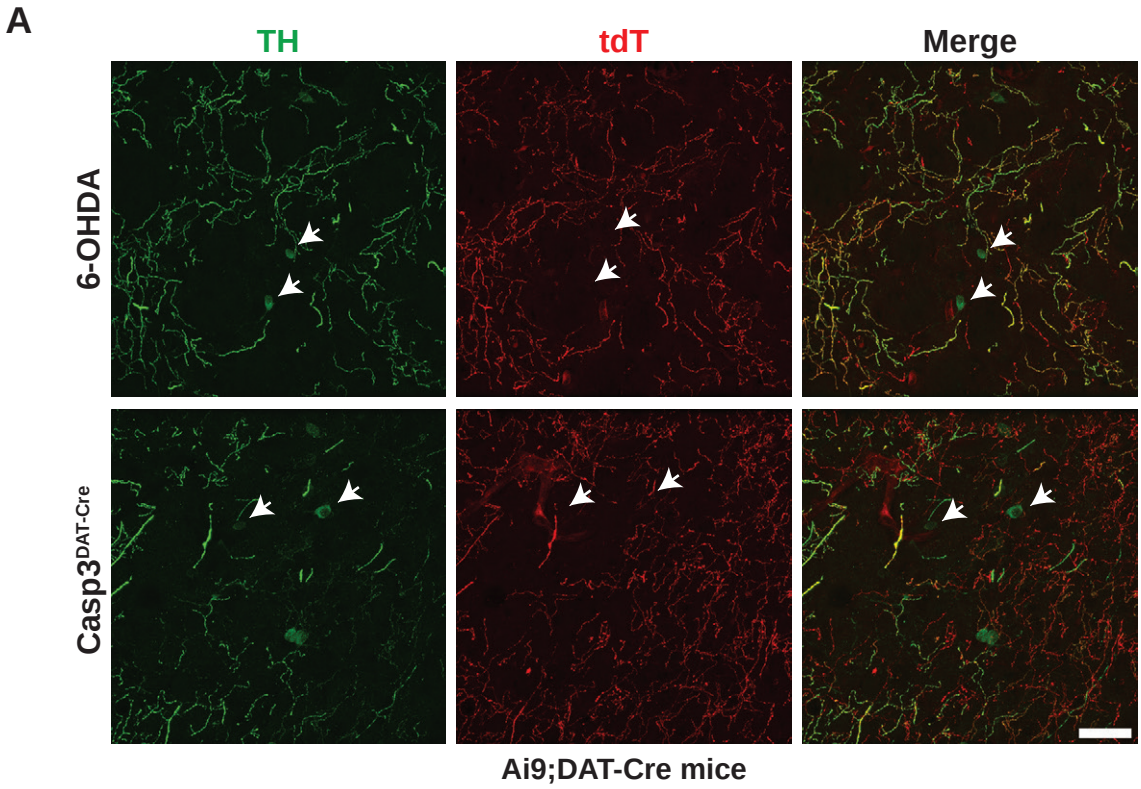

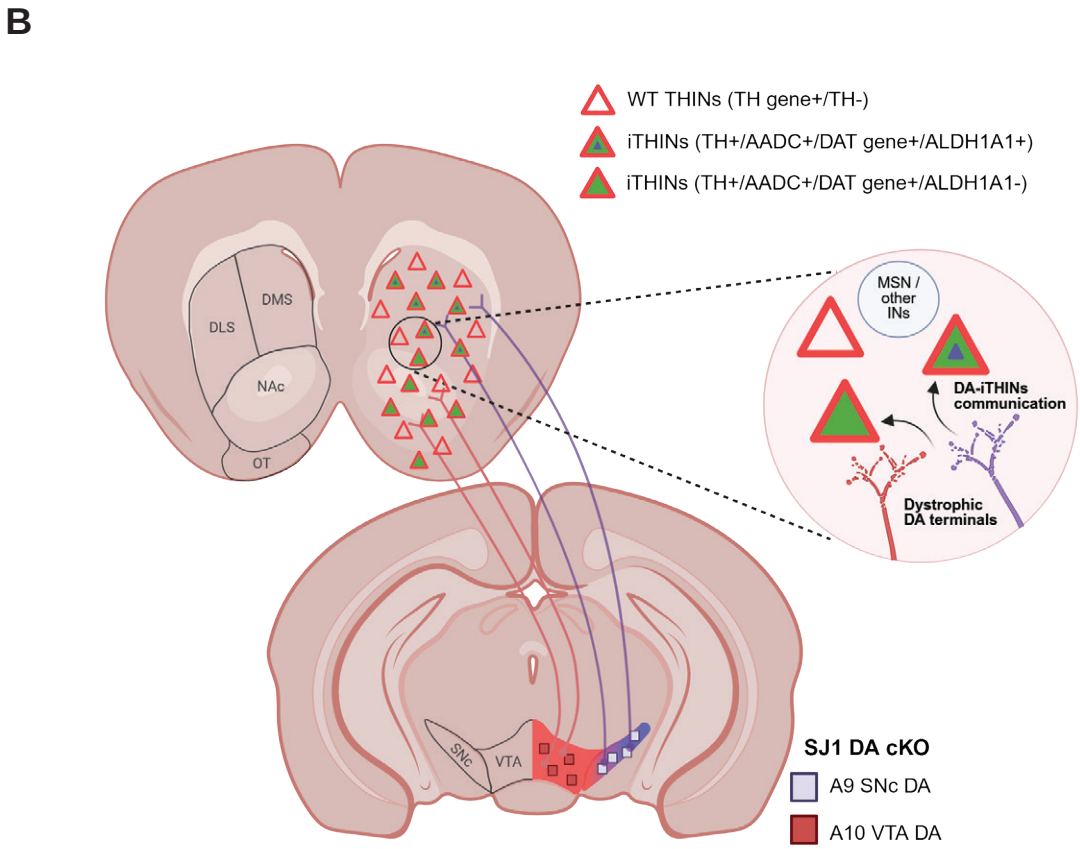

Supplementary Figure 10

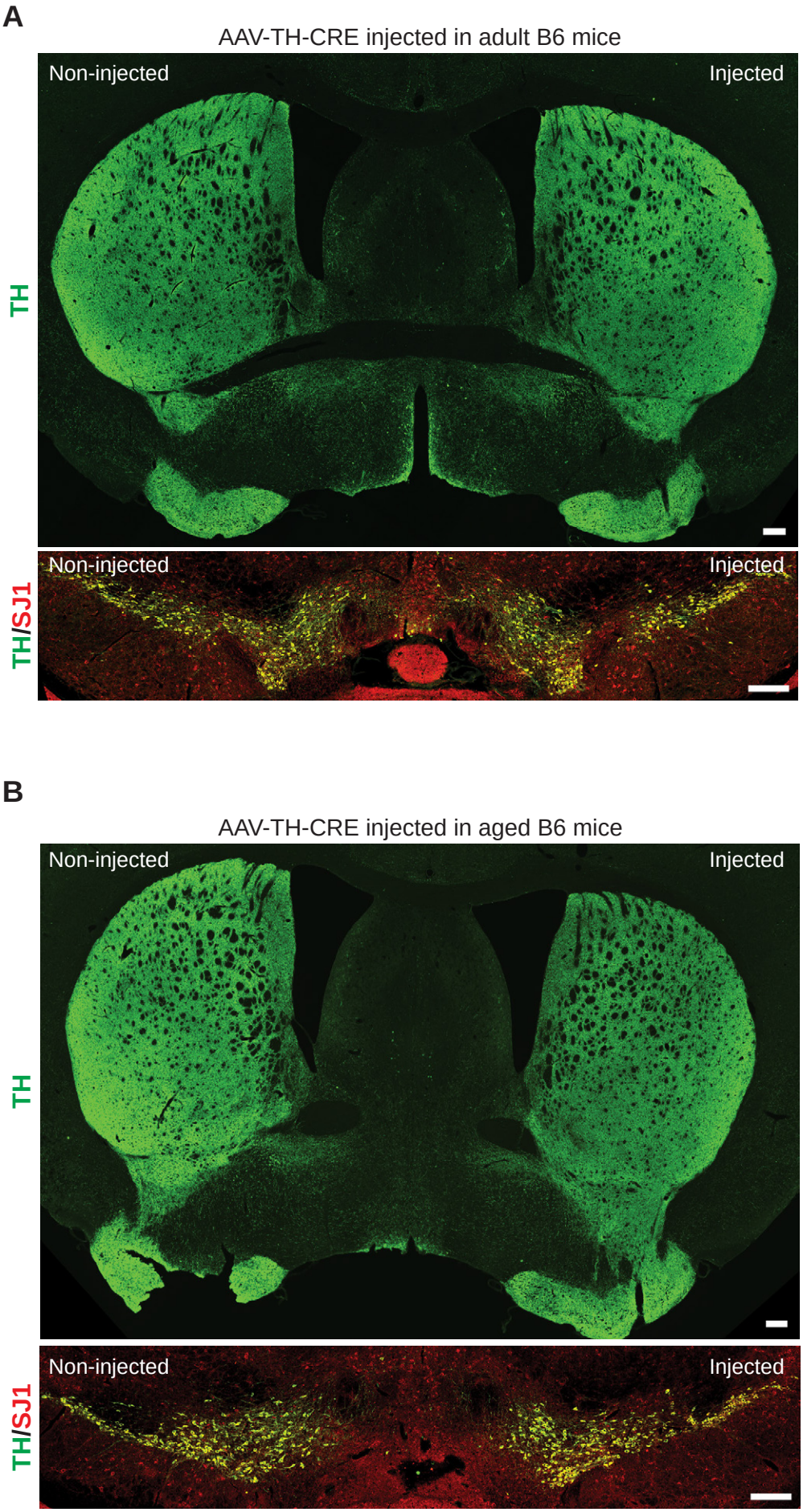

Supplementary Figure 11

Mice Model		*TH*	*AADC*	*ALDH1A1*	*DAT*
Ai9;TH-Cre	WT THINs	- (*TH gene+)	-	-	-
SJ1 cKO^{DAT}	iTHINs	+++	+++	+++ (*subregion)	- (*DAT gene+)
SJ1 cKOTH	iTHINs	+++	+++	+++ (*subregion)	-
6-OHDA model		+	-	-	-
Casp3 model		+	-	-	-

+++ positive and high expression;
+ positive and mild expression;
- negative/cannot be detected with immunostaining;
*remarks

Table S1. Immunostaining of THINs observed in genetic and lesioned mice models